Journal of Biological Engineering

RESEARCH

Open Access

Bioreactor expansion of human neural progenitor cells for exosome scalable production and miRNA-engineering

Miriam Corraliza-Gomez[1,2†], Marta Ianni[1,3†], Diogo E. S. Nogueira[4,5], William O. S. Salvador[4], Mafalda Miguéis[1,8], Monica Garcia-Alloza[2,6], Carlos A. V. Rodrigues[4,7], Joaquim M. S. Cabral[4] and Dora Brites[1,8*]

Abstract

Upscaling protocols to produce exosomes from human neural precursor cells (NPCs) are crucial for enabling broader therapeutic applications for neurodegenerative diseases with associated inflammation. Exosomes are small extracellular vesicles measuring between 30 and 150 nm in diameter that are emerging as promising delivery systems in cell-free therapies. An analysis of the US-NIH clinical trials database identifies 246 studies focused on exosome diverse applications, underscoring the growing importance of both naïve and engineered exosomes, specifically those enriched with miRNAs. NPC transplantation has faced several challenges, including immunogenicity and limitations associated with the ineffectiveness of single-dose administration. However, NPC exosomes are emerging as more promising therapeutic tools due to the possibility of multiple applications and their unique properties such as low immunogenicity, biocompatibility, ability to penetrate biological barriers and neuroregenerative properties. To tackle the challenge of producing large quantities of high-quality exosomes, our research used advanced three-dimensional cultivation techniques in vertical-wheel (PBS) and stirred-tank (DASbox) bioreactors. Bioreactor-upscaled ReNcell® VM human NPCs enhanced exosomal yield while maintaining essential stem NPC characteristics. DASbox bioreactor produced smaller, more uniformly sized neurospheres than the PBS system. DASbox-generated exosomes demonstrated superior transfection efficiency with pre-miR-124-3p, here used as a promising neuroprotective strategy, and improved microglia uptake than those from PBS or adherent cultures. Moreover, DASbox-derived exosomes were shown to be internalized by neurons and glial cells and to differently regulate inflammatory mediators upon stress conditions, while exerting better modulatory activity when transfected with pre-miR-124-3p. These results highlight the potential of exosomes from bioreactor-upscaled human NPCs as innovative therapeutic agents for targeting neuron-glia dyshomeostasis and dysfunctional miRNAs in neurodegenerative diseases, meeting the growing demand for their therapeutic application and supporting the development of more effective strategies.

†Miriam Corraliza-Gomez and Marta Ianni contributed equally to this work.

*Correspondence:
Dora Brites
dbrites@ff.ulisboa.pt

Full list of author information is available at the end of the article

© The Author(s) 2025. **Open Access** This article is licensed under a Creative Commons Attribution-NonCommercial-NoDerivatives 4.0 International License, which permits any non-commercial use, sharing, distribution and reproduction in any medium or format, as long as you give appropriate credit to the original author(s) and the source, provide a link to the Creative Commons licence, and indicate if you modified the licensed material. You do not have permission under this licence to share adapted material derived from this article or parts of it. The images or other third party material in this article are included in the article's Creative Commons licence, unless indicated otherwise in a credit line to the material. If material is not included in the article's Creative Commons licence and your intended use is not permitted by statutory regulation or exceeds the permitted use, you will need to obtain permission directly from the copyright holder. To view a copy of this licence, visit http://creativecommons.org/licenses/by-nc-nd/4.0/.

Keywords Upscaled-exosome production, Neural precursor cells, Cell-free therapies, Vertical-wheel bioreactors, Stirred-tank bioreactors, miRNA-124-engineered exosomes, Paracrine signaling

Graphical Abstract

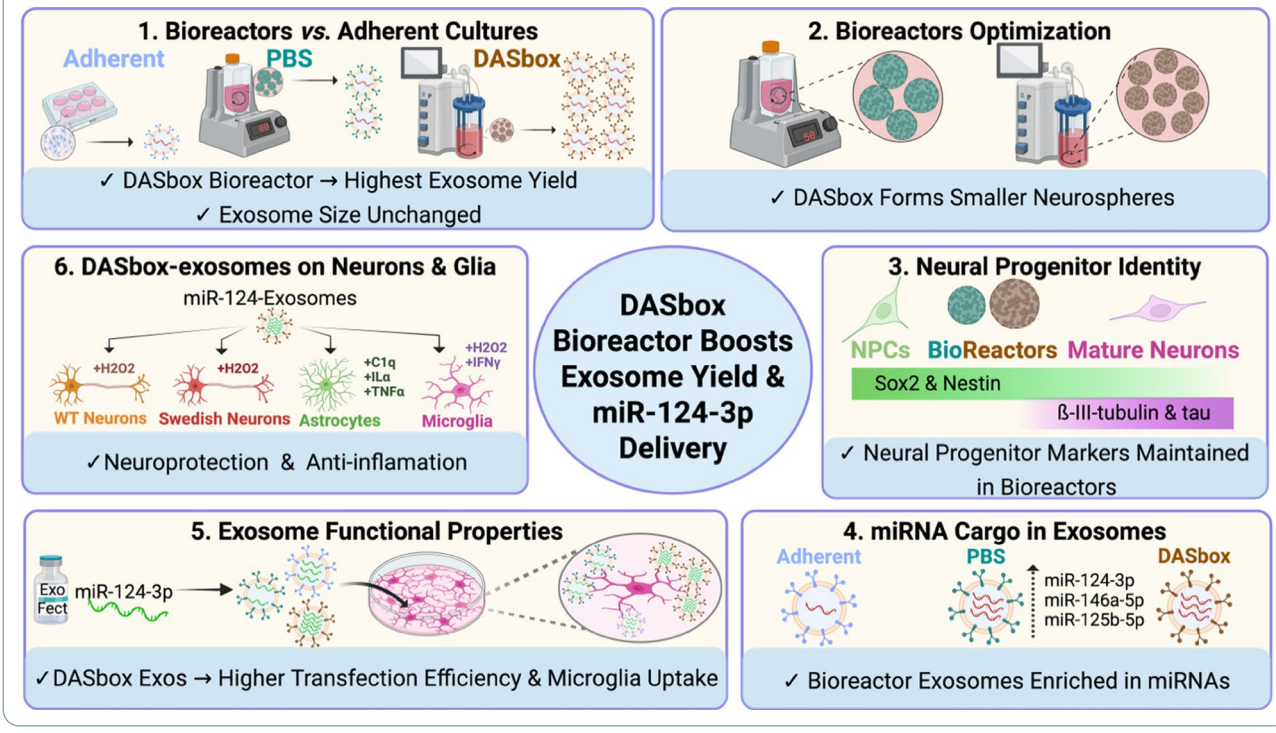

Background

All living cell types release extracellular vesicles (EVs), which are lipid bilayer-delimited particles not containing a functional nucleus and ranging from nano- to micro-sizes [1]. When using lower size cut-off membranes during the isolation process by differential ultracentrifugation, small extracellular vesicles (sEVs) with diameters < 200 nm are collected [2]. Such sEVs, despite not being characterized as having subcellular origin, are currently named in the literature as exosomes [3] and have been increasingly recognized as effective cargo delivery systems in cell-free therapeutics [4]. The US-NIH clinical trials database highlights the growing significance of exosomes, reporting 246 studies encompassing various stages of research, including completed, recruiting, and suspended trials (https://clinicaltrials.gov/search?cond=exosomes). Biotech companies typically utilize either naïve exosomes, which are naturally produced by cells, or engineered exosomes, which are loaded with nucleic acids or other biomolecules [5]. A crucial consideration in the development of exosome-based therapies is the selection of cells that will produce the exosomes for potential clinical application. In this regard, neural stem cells (NSCs) are a promising option. These multipotent stem cells are found in regions of the brain such as the olfactory bulb, subventricular zone, and hippocampus, and they possess the potential to self-renew and differentiate into neurons, astrocytes, and oligodendrocytes [6]. NSCs have demonstrated therapeutic potential after transplantation, primarily through their secretion of neuroprotective and immunomodulatory compounds, enhancing synaptogenesis, and replacing degenerating or damaged neurons [7, 8]. However, NSCs face limitations, including insufficient differentiation and integration post-transplantation, as well as certain immunogenicity characteristics. Additionally, their application is restricted to a single administration, which poses challenges for broader clinical use [9, 10]. In contrast, NSCs-derived exosomes can be used in multiple treatments and offer several advantages. They exhibit low immunogenicity, a high capacity to cross the blood-brain barrier and notable neuroregenerative abilities, besides having stable physical and chemical properties, and no ethical concerns, which collectively makes them a compelling strategy for treating neurodegenerative diseases [11, 12]. Importantly, NSC-EVs are not phagocytosed or degraded by mononuclear phagocytes, further enhancing their therapeutic potential [13]. Furthermore, exosomes from NSCs can themselves regulate the differentiation of other NSCs, enhancing their potential as a cell-free therapy for neurodegenerative diseases [14, 15].

However, an important challenge in the biomedical application of exosomes is the production of large quantities of high-quality vesicles. Conventional two-dimensional (2D) adherent cultures offer limited growth area per volume, resulting in low yields of exosomes. In contrast, three-dimensional (3D) cultivation using bioreactors provides a more physiologically representative environment, allowing for easier control and real-time monitoring while facilitating scalable processing [16]. For instance, the PBS 0.1 Mini vertical-wheel bioreactor combines both radial and axial flow components, promoting the formation of a high volume of viable cell aggregates in suspension while maintaining the pluripotent quality of the cells [17, 18]. Bioreactors are considered a promising platform to address the challenges associated with scaling up the production of induced pluripotent stem cells (iPSCs) [19], as well as NSCs and neural progenitor cells (NPCs) [20, 21]. When expanding NPC spheres, the agitation in these bioreactors can be finely regulated to control neurosphere size and minimize necrosis within the center of such aggregates [22]. The horizontal DASbox® Mini bioreactor system is also effective for producing a high number of neurospheres while preserving exosome quality. This system, equipped with an 8-blade 60°-pitch impeller, enables precise control over pH, dissolved oxygen, and temperature, resulting in a homogeneous aggregate suspension of human iPSCs with diameters ranging from 150 to 350 µm by day 7 of the process, depending on the specific cell line [23]. In addition, a recent study demonstrated that culturing human mesenchymal stromal cells (MSCs) in the PBS bioreactor yields 2.5-fold more EVs and upregulates the expression of several microRNAs (miRNAs), along with proteins related to metabolism, autophagy, and reactive oxygen species, compared to EVs produced in 2D cultures [24]. This upscaled production of exosomes is crucial for applications in cell-free therapeutics for neurodegenerative diseases.

Building on the promising characteristics of NSC-derived exosomes, our study aimed to upscale their production to be used as carriers for miRNA-124-3p therapeutic applications [25]. Indeed, our recent studies have demonstrated that miR-124 suppresses the production of the amyloid precursor protein (APP), preserves dendritic spines and exerts anti-inflammatory effects in human and mouse models of Alzheimer's disease (AD) [2, 26, 27], while other studies have shown that it inhibits beta-secretase 1 (BACE1), reduces tau hyperphosphorylation, and promotes a neuroprotective microglial phenotype [28–30]. In conformity, we hypothesized that NSC-derived exosomes transfected with pre-miR-124-3p could serve as an efficient and functional delivery system for neuroregenerative applications. Notably, loading pre-miR-124-3p in exosomes from umbilical cord blood mononuclear cells and from SH-SY5Y neuroblastoma cells has already revealed therapeutic potential in experimental models of Parkinson's and Alzheimer's diseases, respectively [2, 31]. The advantage of using exosomes from NSCs reside in their own neuroregenerative potential [32], due to their cargo in growth factors [33] and in miRNAs with renewing potential [34].

In this study, we aimed to compare the efficacy of two bioreactor systems in (1) sustaining the stem cell properties of human ReN-VM cells and (2) producing higher sEVs yield compared with 2D adherent cultures. To the best of our knowledge, we were pioneers in evaluating the content of these ReN cell-derived sEVs in selected inflammatory miRNAs and their potential for miR-124-3p transfection. Our goal was to establish the neuroprotective and anti-inflammatory benefits of these miR-124-3p-loaded ReN-exosomes in regulating the miR-124-3p content of neurons, astrocytes and microglial cells leading to cell-type-specific modulation of inflammation-related genes over naïve exosomes. Further elucidation of the therapeutic benefits of these miR-124-3p enriched sEVs on neuro-immune dyshomeostasis and amyloid plaque formation levels is being conducted in the 5xFAD, a common model of AD [35], as a new therapeutic strategy to be translated into the clinics for improving outcomings in patients with AD.

Methods

Human ReN VM cell monoculture and differentiation

The ReNcell® VM human neural progenitor cell line (NPC, Merck, Darmstadt, Germany), derived from the ventral mesencephalon of a human fetal brain, can differentiate into neurons and glial cells [36]. ReN cells were maintained at 37 °C in a 5% CO_2 humidified atmosphere under adherent conditions in poly-ornithine (15 µg/mL; Sigma-Aldrich, St. Louis, MO, USA) and laminin (10 µg/mL; Thermo Fisher Scientific, Waltham, MA, USA) coated flasks, using Dulbecco's Modified Eagle's Medium/Nutrient Mixture F-12 (DMEM/F-12, Gibco, Thermo Fisher Scientific), supplemented with 1% L-glutamine (Thermo Fisher Scientific), 1.6 g/L D-glucose (final concentration 4.75 g/L), 1% penicillin/streptomycin (P/S, Gibco, Thermo Fisher Scientific), 1% N2 (Gibco), insulin (20 µg/mL, Sigma-Aldrich), B27 (20 µL/mL, Gibco), epidermal growth factor (EGF, 20 ng/mL, PeproTech), and fibroblast growth factor (FGF, 20 ng/mL, PeproTech). The entire culture medium was replaced with fresh medium every 48 h, with B27, EGF and FGF freshly added. Cells were detached using accutase (Gibco) for 7 min at 37 °C, then diluted in culture media, mechanically dissociated into single cells, centrifuged (200 g, 3 min), and resuspended in culture media. Viability was assessed via trypan blue exclusion in a Neubauer chamber, and cells were maintained at 100,000 cells/mL in 25 mL-flasks, making a seeding density of ~ 4,000 cells/cm^2.

For undifferentiated adherent experiments, ReN cells were seeded at 250,000 cells/mL in 6-well plates, which corresponded to ~26,000 cells/cm². For neuronal differentiation, cells were seeded at 25,000 cells/cm² in coated flasks with complete medium. Growth factors (EGF and FGF) were removed the following day to induce differentiation, and cells were cultured for 14 days with complete medium refreshed every 2–3 days.

Bioreactor culture of human ReN VM neurospheres

Undifferentiated ReN cells were inoculated at 250,000 cells/mL in either a PBS 0.1 Mini Vertical-Wheel Bioreactor (PBS BioTech, Camarillo, CA, USA) or a DASbox® Mini Bioreactor System (Eppendorf, Hamburg, Germany). The PBS 0.1 bioreactor had a 60 mL working volume, with 15×10^6 cells initially seeded and agitation maintained at 50 rpm throughout the experiment. The DASbox bioreactor had an 80 mL working volume, with 20×10^6 cells seeded. To minimize shear stress, agitation in the DASbox system gradually increased from 20 rpm (first hour) to 60 rpm (first 24 h) and then to 100 rpm for the remainder of the experiment. In addition, in the DASbox system bioreactor conditions were tightly controlled, with pH maintained at 7.2, temperature at 37 °C and dissolved oxygen set at 100% air saturation. In both systems, 80% of the culture media was replaced every 48 h.

Samples (1 mL) were collected daily under agitation, and the aggregates (neurospheres) were analyzed using an inverted microscope (Leica DMI3000B/Nikon Digital Camera Dxm1200F). Aggregate size was measured as previously described [18]. Samples were centrifuged (200 g, 3 min), and aggregates were dissociated with accutase for single cell counting in a Neubauer chamber to assess proliferation. Supernatants were centrifuged (300 g, 10 min) to pellet debris and then stored at -80 °C until exosome isolation.

Isolation and characterization of ReN cell-derived exosomes

Exosomes were isolated from collected media via differential ultracentrifugation, as we previously described, using a lower size cut-off membrane [37]. Briefly, the conditioned media were first centrifuged (1,000 g, 10 min, 4 °C) to remove cell debris. Supernatants were then centrifuged (16,000 g, 60 min, 4 °C) to pellet large EVs (250–1000 nm diameter). The remaining supernatant was filtered (0.22 µm pore size) and ultracentrifuged (100,000 g, 2 h, 4 °C) using a Beckman Optima™ L100 XP Ultracentrifuge with a 90Ti fixed-angle rotor (Beckman Coulter, Spain) to isolate the sEVs, mostly exosomes, as we published previously [37, 38].

Exosomes isolated following this procedure in our laboratory has evidenced the characteristic Alix, Flotilin-1 and CD63 proteins and a cup-shaped morphology when observed by transmission electron microscopy [37]. High-plex profiling of exosome lysates, recently done for a manuscript to be submitted for publication, revealed that > 90% of proteins are sustained from the exosomes isolated from static cultures to those obtained by bioreactors and not affected by the miR-124-3p transfection (data not shown). Pellets were resuspended in Dulbecco's Phosphate-Buffered Saline (DPBS) for nanoparticle tracking analysis (NTA) or in QIAzol for RNA extraction. Exosome size and concentration were assessed by NTA using a NanoSight NS300 (Malvern Instruments, U.K.), with samples automatically injected using an O-Ring Top Plate. For each sample, five 60 s videos were recorded and analyzed with NTA 3.2 software.

All exosome preparations were used immediately after isolation, without undergoing freeze–thaw cycles, in order to preserve vesicle integrity and functional cargo, in line with the recommendations of the MISEV2023 guidelines [1].

PKH labeling of ReN cell-derived exosomes

Exosomes were labeled with the lipophilic dye PKH26 Red Fluorescent Cell Linker (Sigma-Aldrich) to track cellular targeting and biodistribution. Exosomes were isolated and resuspended in DPBS, with the volume adjusted to 1 mL using Diluent C. Then, 6 µL of PKH26 dye was added, achieving a final concentration of 6 µM. The mixture was gently pipetted for 30 s and incubated for 5 min at room temperature. To stop the staining, DPBS was added to bring the volume to 8.5 mL, followed by ultracentrifugation at 100,000 g for 2 h at 4 °C to remove excess dye. Pellets were resuspended in DPBS for quantification and DMEM for delivery.

Transfection of ReN cell-derived exosomes with pre-miR-124-3p

Exosome batches were normalized for number (using NTA) before transfection. ReN-derived exosomes were loaded with pre-miR-124-3p Precursor (Ambion, Austin, TX, USA) using the Exo-Fect™ Exosome Transfection Kit (System Biosciences, Palo Alto, CA, USA) following the manufacturer's protocol. Exosomes were resuspended in DPBS, mixed with Exo-Fect reagent and pre-miR-124-3p (1.66 µM). Non-transfected exosomes received DPBS instead of the pre-miRNA. Transfection occurred at 37 °C for 10 min with manual agitation every 2 min, followed by a 5-min cool-down on ice. ExoQuick-TC Reagent (1:5) was added to stop the process, and the samples were incubated on ice for 30 min. Transfected exosomes were isolated by centrifugation (17,500 g, 30 min), and the exosomal pellet was resuspended in DPBS. Successful loading with miR-124-3p into the exosomes was verified by RT-qPCR.

Culture of SH-SY5Y, CHME3 and IM-HA human cell lines

Cell lines were maintained in T75 flasks in a 5% CO_2 humidified incubator at 37 °C. Culture media were changed every 2 days, and cells were passed on when they reached 80% confluence. To detach cells, trypsin-EDTA 0.05% (Gibco) was used for 3 min at 37 °C, followed by dilution with fetal bovine serum (FBS, Gibco)-containing media and centrifugation (200 g, 5 min).

The SH-SY5Y wild type (SH-*WT*) and those transfected with APP695 (SH-*SWE*) human neuroblastoma cell lines were kindly provided by Professor Anthony Turner [39]. Cells were cultured in DMEM 4.5 g/L D-glucose media, supplemented with 10% FBS and 2% antibiotic/antimycotic (AB/AM, Sigma-Aldrich). For experiments, cells were seeded (22,000 cells/cm^2) in wells coated with poly-D-lysine (100 µg/mL, Sigma-Aldrich) and laminin (4 µg/mL, Gibco) in complete media. Neuronal differentiation was induced with 10 µM retinoic acid (in DMEM containing 2% AB/AM and 1% FBS) for 7 days, with media changes every 2 days.

The CHME3 human microglial cell line was provided by Professor Marc Tardieu [40]. Cells were cultured in DMEM 4.5 g/L D-glucose media (Gibco), supplemented with 10% FBS (Gibco), 2% AB/AM (Sigma-Aldrich), and 1% L-glutamine (Gibco), as usual in our laboratory [26]. For experiments, microglia (30,000 cells/cm^2) were seeded in complete media and, after 24 h, culture media was changed to exosome-depleted 1% FBS, which is obtained by centrifugation at high speeds to eliminate native exosomes [41] and to prevent as much as possible the FBS influence on exosomes [42].

The IM-HA human immortalized astrocyte cell line was obtained from Innoprot (Ref: P10251-IM, Derio, Spain). Cells were cultured in DMEM supplemented with 2% FBS, 2% AB/AM, and 1% N2. For experiments, astrocytes were seeded (26,000 cells/cm^2) in complete media.

Cell internalization of PKH26-labeled exosomes and immunocytochemistry

To compare the internalization of exosomes produced under different culture conditions by CHME3 microglia, cells were seeded on 18 mm coverslips at 21,500 cells/cm^2. Exosomes from ReN cells grown in 2D cultures and 3D bioreactors were PKH26-labeled, quantified by NTA, and an equal number (1.36×10^8 particles/mL) was delivered to microglia in low-serum media.

In a separate experiment, PKH26-labeled DASbox-produced exosomes were delivered to differentiated SH-*WT* and SH-*SWE* neuron-like cells and IM-HA astrocytes seeded on coverslips (26,000 and 39,500 cells/cm^2, respectively). After 24 h, cells were washed, fixed with 4% paraformaldehyde [15 min, room temperature (RT)], permeabilized (0.1% Triton-X100 in PBS, 5 min RT), and blocked (1% BSA in PBS, 30 min RT). Afterwards, immunostaining was performed as follows: F-actin in microglia was stained with AlexaFluor® 647 Phalloidin (1:400, A22287 Invitrogen) for 1 h RT; SH-*WT* and SH-*SWE* neurons were stained with ß-III-tubulin (1:100, MAB1637 Merck) overnight at 4 °C, followed by incubation with goat anti-mouse Alexa Fluor Plus 488 (1:500, A32723 Invitrogen) for 2 h RT; and IM-HA astrocytes were stained with glial fibrillary acidic protein (GFAP, 1:200, orb539616 Biorbyt Ltd., Cambridge, UK) overnight at 4 °C, followed by incubation with goat anti-rabbit Alexa Fluor Plus 488 (1:500, A11008 Invitrogen) for 2 h RT. DAPI (5 µg/mL, Invitrogen) was used to stain cell nuclei.

Samples were mounted with Fluoromount Aqueous Mounting Medium (Sigma-Aldrich) and visualized on a Zeiss LSM 900 Airyscan 2 Confocal Microscope (Zeiss). Images were acquired under the same conditions of illumination, diaphragm and condenser adjustments, exposure time, background correction and color levels. Images were analyzed using FIJI software and the EVAnalyzer plugin [43].

Delivery of pre-miR-124-3p transfected exosomes to microglia, astrocytes and neurons

To compare transfected exosomes' ability to modulate miR-124-3p levels in microglia, CHME3 cells were seeded at 21,500 cells/cm² in 12-well plates. Exosomes from ReN cells grown in 2D or 3D cultures were isolated and Exo-Fect™ transfected with pre-miR-124-3p, quantified by NTA, and an equal number (1.86×10^7 particles/mL) was delivered to microglia in low-serum media. After 24 h, cells were washed with PBS, collected and lysed using QIAzol Lysis Reagent (QIAGEN, Hilden, Germany).

For functional effects on neurons, astrocytes, and microglia under stress, each cell type was exposed to stressors for 24 h, followed by exosome treatment for 24 h maintaining the stressor agents. Neurons were stressed with 10 µM hydrogen peroxide (H_2O_2, Merck) and treated with naïve or pre-miR-124-3p transfected exosomes (1.15×10^7 particles/mL). Astrocytes were treated with the Liddelow cocktail — IL-1α (3 ng/mL, PeproTech), TNF-α (30 ng/mL, Cell Signaling Technology, Danvers, MA, USA) and C1q (400 µg/mL, MyBioSource Inc., San Diego, CA, USA) to induce a reactive phenotype and treated with exosomes, as before. Microglia were stressed with interferon-gamma (IFN-γ, type II IFN; 10 ng/mL, Bachem, Switzerland) and H_2O_2 (10 µM) and similarly treated with exosomes as indicated for neurons and astrocytes. After incubation, cells were washed, collected and lysed using TRIzol Reagent (Invitrogen).

Table 1 miRNAs analyzed by RT-qPCR

miRNAs	Target Sequence (5'-3')
hsa-miR-124-3p	UAAGGCACGCGGUGAAUGCC
hsa-miR-146a-5p	UGAGAACUGAAUUCCAUGGGUU
hsa-miR-125b-5p	UCCCUGAGACCCUAACUUGUGA
hsa-miR-21-5p	UAGCUUAUCAGACUGAUGUUGA
hsa-miR-155-5p	UUAAUGCUAAUCGUGAUAGGGGU
hsa-U6	Reference Gene

hsa, *homo sapiens*; miR, miRNA; RT-qPCR, reverse transcription-quantitative polymerase chain reaction.

Table 2 Genes analyzed by RT-qPCR

Gene	Primer sequence (5'-3')	Amplicon size (bp)
FABP7	Fwd: GGCTTTGCCACTAGGCAGG Rev: TGACCACTTTGTCTCCTTCTTGA	76
RAGE	Fwd: GCCACTGGTGCTGAAGTGTA Rev: GTCCGGCCTGTGTTCAGTTT	78
RPL18	Fwd: GTCCCTTTCCCGGATGAT Rev: GACAGTGCCACAGCCCTTAG	229
STAT3	Fwd: ACCAGCAGTATAGCCGCTTC Rev: GCCACAATCCGGGCAATCT	124

RT-qPCR, reverse transcription-quantitative polymerase chain reaction; FABP7, gene that encodes for fatty acid binding protein 7; RAGE, gene that encodes for the receptor for advanced glycation end products; RPL18, gene that encodes the ribosomal protein L18; STAT3, gene that encodes the signal transducer and activator of transcription 3; Fwd, forward; Rev, reverse; bp, based pairs.

RNA extraction from cells and exosomes

Total cellular RNA was extracted following the manufacturer's protocol. Briefly, lysed cells in TRIzol were mixed with chloroform (1:5), vigorously homogenized, and centrifuged (12,000 g, 15 min, 4 °C). The aqueous phase containing RNA was collected, mixed with an equal volume of isopropanol, and incubated overnight at -20 °C for small RNA precipitation. Samples were then centrifuged (10,000 g, 10 min, 4 °C), and RNA pellets were washed with 70% ethanol at -20 °C for 1 h. After a final centrifugation (12,000 g, 15 min, 4 °C), ethanol was discarded, and RNA pellets were air-dried for 15 min at RT before resuspension in nuclease-free water.

Exosomal miRNAs were extracted using the miRNeasy Micro Kit (QIAGEN) according to the manufacturer's protocol. Exosomal pellets were resuspended in QIAzol, incubated for 5 min at room temperature, and mixed with chloroform (1:5). After centrifugation (12,000 g, 15 min, 4 °C), the aqueous phase was collected, mixed with 1.5 volumes of ethanol, and transferred to a RNeasy Mini Column. RNA was bound to the silica membrane, contaminants were removed through sequential washes with kit-specific buffers, and finally RNA was eluted in RNase-free water.

RNA concentration and purity were assessed using the NanoDrop ND-1000 Spectrophotometer (NanoDrop Technologies, Thermo Fisher Scientific).

To assess the exosomal-to-cellular miRNA ratio, we pooled equal amounts of 4 biological replicates from independent cell cultures or exosome preparations to generate a single representative sample per condition. This approach allowed for sufficient RNA input to perform comparative RT-qPCR analysis of miRNA levels in both cellular and exosomal fractions within the same experiment.

Reverse transcription and RT-qPCR for miRNAs

cDNA was synthesized using the miRCURY LNA RT Kit (QIAGEN) following the manufacturer's instructions, with a final RNA concentration of 1 ng/µL. The reaction consisted of 60 min at 42 °C, followed by 5 min at 95 °C. RT-qPCR was performed using Power SYBR Green PCR Master Mix (Applied Biosystems, Thermo Fisher Scientific) on a QuantStudio 7 Flex Real-Time PCR System (Thermo Fisher Scientific) under the following conditions: 95 °C for 10 min, then 50 cycles of 95 °C for 10 s and 60 °C for 1 min. Analyzed miRNAs are listed in Table 1. Specificity was confirmed by melting curve analysis (60 °C to 95 °C, 1.6 °C/s ramp), and quantification followed the ΔΔCt method [44].

Reverse transcription and RT-qPCR for genes

cDNA was synthesized using Xpert cDNA Synthesis SuperMix (GRiSP, Porto, Portugal) following the manufacturer's instructions, with a final RNA concentration of 50 ng/µL. RT-qPCR was performed using XPert Fast SYBR 2X MasterMix (GRiSP) on a QuantStudio 7 Flex System. Primers were designed with PrimerBlast (NCBI) or selected from PrimerBank, with a final concentration of 250 nM. *RPL18* served as the housekeeping gene. Analyzed genes are listed in Table 2. The PCR program consisted of an initial denaturation at 95 °C (1.9 °C/s ramp, 2 min hold), followed by 50 cycles at 95 °C for 5 s and 62 °C for 30 s. Specificity was confirmed by melting curve analysis, and quantification followed the ΔΔCt method.

Protein extraction and Western blot

For cell characterization, ReN cells (2D cultures) and neurospheres (3D by bioreactors) were collected in Cell Lysis Buffer (Cell Signaling Technology), supplemented with 0.05 M dithiothreitol and Protease Inhibitors (Sigma-Aldrich), and incubated on ice for 30 min. Then, protein concentration was determined by the BCA™ Protein Assay Kit (Thermo Fisher Scientific). Protein extracts (30 µg) were mixed with protein sample buffer [63 mM Tris-HCl pH 6.8, 10% (v/v) glycerol, 2% (w/v) SDS, 5% (v/v) β-mercaptoethanol, 0.05% (w/v) bromophenol blue], denatured (70 °C, 5 min) and separated on 4–15% Mini-PROTEAN TGX Precast Protein Gels (Bio-Rad Laboratories, Madrid, Spain) at constant voltage (200 V) in electrophoresis buffer [25 mM Tris, 190 mM glycine, 1% SDS, pH 8.3]. Proteins were then transferred to Polyvinylidene Fluoride (PVDF) membranes (Bio-Rad,

Spain) using an immersion system at constant amperage (400 mA, 90 min). Membranes were washed with Tris-buffered saline-Tween 0.1% (TBS-T), blocked with blocking solution (WesternBreeze®, Invitrogen) for 1 h at RT, and incubated overnight at 4 °C with primary antibodies: Mouse anti-ß-III-tubulin (1:500; 2 µg/mL; MAB1637 Merck), Rabbit anti-Sox2 (SRY-box transcription factor 2) (1:500; Biorbyt); Mouse anti-nestin (1:500, 1 µg/mL; Biorbyt); Rabbit anti-Tau (1:2000; A0024, Dako, Agilent Technologies, Denmark); Mouse anti-ß-actin (1:2000; 1 µg/mL; A1978 Sigma-Aldrich). Alkaline phosphatase-conjugated secondary antibodies (WesternBreeze™) were used, and membranes were developed with Novex AP chemiluminescent substrate (WesternBreeze™). Signals were captured using a digital camera (ChemiDoc MP; Bio-Rad). Membranes were stripped using a Stripping buffer solution (Alfa Aesar, Thermo Fisher Scientific) following manufacturer's instructions. Immunoblots were analyzed semi-quantitatively by measuring the integrated optical density of the immunoreactive protein bands in images taken within the linear range of the camera, avoiding signal saturation and using ImageJ software. Each band was normalized to β-actin.

To characterize and compare exosomes derived from ReN cells in 2D cultures and 3D bioreactors, sEVs were isolated as described previously and resuspended in 40 µL of lysis buffer (50 mM Tris-HCl pH 7.4, 180 mM NaCl, 1mM EDTA, 1% Triton X100) supplemented with protease inhibitors (Sigma-Aldrich). Samples were sonicated (3 cycles of 15s sonication and 30s ice) and centrifuged at 12,000 rpm, 15 min at 4º C. The supernatant was collected, and protein concentration was determined using the MicroBCA Protein Assay Kit (Thermo Scientific™). 20 µg of cell and exosomal protein were mixed with Fluorescent Compatible Sample Buffer 4x (Invitrogen), denatured (95 °C, 5 min) and separated on a 6–20% gradient gel at constant current (30 mA). Proteins were then transferred into PVDF membranes using the iBlot 3 Western Blot Transfer System (Thermo Scientific™) at constant voltage (27 V) for 7 min, under medium cooling conditions. The membranes were incubated with No-Stain Protein Labeling Reagent (Thermo Scientific™) for 20 min at RT and visualized using the iBrightTM FL1500 Imaging System, at 488 nm. Membranes were then blocked using Immobilon Fluorescent Blocker (Thermo Scientific™) for 1 h at RT and then incubated overnight at 4 °C with primary antibodies diluted in SignalBoost™ Immunoreaction Enhancer Kit solution 1 (Millipore). The following primary antibodies were used: mouse-anti-Alix (1:500, #2171S, Cell Signalling), mouse anti-Flotillin (1:500, #610820, BD-Biosciences), mouse anti-CD63 (1:500, sc-5275, Santa Cruz Biotechnology), rabbit anti-GAPDH (1:500, #ABS16, Millipore). Membranes were washed with TBS-T and incubated for 2 h at RT with fluorophore-conjugated secondary antibodies diluted in the SignalBoost™ Immunoreaction Enhancer Kit solution 2. The following secondary antibodies were used: Goat anti-Mouse IgG (H + L) Alexa Fluor™ 750 (1:1000) and Goat anti-Rabbit IgG (H + L) Alexa Fluor™ 594 (1:1000). Membranes were washed with TBS-T, dried, and imaged using the iBrightTM FL1500 Imaging System.

Statistical analysis

Statistical analyses were performed with GraphPad Prism 9 (GraphPad Software Inc., San Diego, CA, United States) and RStudio (RStudio Team, version 2024.12.1 + 563). Data are represented as mean ± Standard Error of the Mean (SEM) of at least three independent experiments. Outliers were identified and removed using the ROUT method (Q = 1%) to ensure the reliability and precision of the statistical analyses. Statistical comparisons between two groups were made by using *t*-test, while multiple groups were compared using one-way or two-way ANOVA, depending on the number of factors, with Tukey's post-hoc test to assess statistical significance between groups. A significance threshold of $\alpha = 0.05$ was used for hypothesis testing. Specific statistical tests for each experiment are detailed in the respective Figure legend. Heatmap and hierarchical clustering were performed using the *pheatmap* package [45].

Results

Upscaling of ReN cells and their derived exosomes is better by the DASbox bioreactor than by the other tested alternatives, without modification of their vesicle size diameter

Exosome size varies with isolation methods, cell origin, and characterization techniques [46]. While MSC-derived exosomes show consistent diameters across small-scale flasks and large-scale bioreactors [47], efficient clinical translation also requires cost-effective large-scale production. Bioreactors were shown to produce about six times more vesicles than static cultures, while maintaining vesicle's integrity, reproducibility, homogeneity from batch to batch and preserving biological activity [16], but their impact on vesicle size remains unclear. Since our previous experience was only with exosomes isolated from static 2D cultures [37, 38, 48], here we assessed whether large-scale production of 3D neurospheres increases exosomal yield and affects vesicle size, when compared with adherent cell cultures.

Human ReN cells were cultured using three different conditions: 2D cultures with poly-ornithine/laminin coating, 3D-neurospheres in the PBS-Mini 0.1 bioreactor and 3D-neurospheres in the DASbox bioreactor (Fig. 1A), all seeded at 250,000 cells/mL. Key differences among the three culture systems were: (i) the amount of media required; (ii) the culture type, with the 2D system being

adherent, therefore producing a monolayer, while the 3D systems were suspension-based, resulting in cellular aggregates; and (iii) the agitation, which was absent in the 2D culture, vertical (50 rpm) in the PBS 0.1, and horizontal (100 rpm) in the DASbox. Unlike PBS, the DASbox is operated externally, with continuous monitoring and adjustment of critical parameters for cell growth, including pH, dissolved oxygen and temperature, using specific sensors. Morphologically, 2D cultures formed adherent monolayers, whereas both bioreactor systems promoted 3D aggregation (Fig. 1B).

After 48 h in culture, ReN cell doubling times were similar in adherent and DASbox conditions (77.0 ± 15.7 h *vs.* 73.4 ± 4.3 h, respectively), but slightly longer in PBS bioreactors (115.4 ± 51.9 h), likely due to reduced aggregability during the initial 24 h. Despite these differences, cell proliferation was comparable across systems, as indicated by similar cell concentrations at harvest (Fig. 1C). ReN cells produced and released exosomes under all conditions, but slightly more efficiently in the DASbox condition (Fig. 1D), when exosome yield was normalized to the number of cells to assess secretory efficiency, potentially due to improved cell-to-cell interactions or more physiologically relevant culture conditions. Exosome concentration in the conditioned media was also quantified, with the DASbox bioreactor producing approximately 1.5 times more exosomes per mL (not statistically significant) than adherent or PBS bioreactor cultures (Fig. 1E). To evaluate the total production capacity of each system, we calculated the absolute exosome yield by multiplying the exosome concentration (particles/mL) by the total culture volume. This revealed more than a 120-fold increase in total exosome output in the DASbox bioreactor compared to adherent cultures ($p < 0.01$), as depicted in Fig. 1F.

To confirm the identity and purity of isolated vesicles, exosome and cell lysates were analyzed by Western blot (Fig. 1G). Exosomal preparations from both 2D and 3D cultures were enriched in canonical exosome markers such as Alix and CD63, confirming successful isolation of *bona fide* exosomes. Consistent with these findings, exosome size distribution analyzed by NTA was similar across conditions, extending mainly between 50 and 220 nm and peaking around 150 nm (Fig. 1H). The distribution appeared to be unimodal, indicating a relatively homogeneous population of exosomes, with slight variability. The average diameter of exosomes was close to 190 nm for adherent cultures, 189 nm for the PBS 0.1 bioreactor, and 170 nm for the DASbox, with no statistically significant differences (Fig. 1I). Overall, the DASbox bioreactor proved to be the most efficient among the tested systems for large-scale production of ReN-exosomes while maintaining their characteristic size and molecular features essential for propagation and cellular uptake.

DASbox bioreactor produces smaller size ReN VM neurospheres and higher exosome yield than the PBS system

After confirming that PBS and DASbox bioreactors significantly increase exosome production over 2D cultures, we evaluated and optimized ReN cell growth in these systems (Fig. 2A). To this end, we analyzed proliferation kinetics and neurosphere diameter, using 60 mL of working volume in PBS and 80 mL in DASbox bioreactors. Minimum stirring speeds to maintain the aggregate suspension were 50 rpm (PBS) and 100 rpm (DASbox) in bioreactors, with lower speeds resulting in aggregate sedimentation. With these settings, 85% of cells had aggregated 24 h post-inoculation, forming viable structures for up to 6 days in culture. Reproducibility was demonstrated across three independent bioreactor runs, with consistent exponential growth kinetics reflected in the average growth curves presented in Fig. 2B. At six days, maximum cell densities reached $0.8 \pm 0.5 \times 10^6$ cells/mL in PBS and $1.0 \pm 0.4 \times 10^6$ cells/mL in DASbox bioreactors. Glucose levels remained above 40% of initial concentration, and lactate never exceeded 16 mM in culture media.

By day 6, the average diameter of cell aggregates gradually increased, reaching 852.3 ± 35.7 µm in the PBS system and 452.4 ± 9.7 µm in the DASbox bioreactor (Fig. 2C). Notably, DASbox-produced neurospheres were more uniform in size and consistently smaller than those from the PBS system throughout the study (Fig. 2D). Smaller aggregates in the DASbox system might enhance nutrient diffusion and waste exchange due to their larger surface area relative to their volume, which may contribute to increased exosome and growth factor production. Overall, smaller aggregates could boost metabolic efficiency and yield, meaning that there is a link between aggregate size, nutrient distribution, and cellular function, an issue that deserves further studies.

To assess exosomal yield, bioreactors were monitored daily for exosome production. Exosome output was similar in both bioreactors, but DASbox showed a noticeable increase from day 3 onward (Fig. 2E). To estimate overall productivity while avoiding absolute values, final exosome yield was expressed as exosome number/mL at the end of the bioreactor run for each system. Although not statistically significant, the DASbox bioreactor tended to produce a higher cumulative yield (Fig. 2F).

Neural differentiation markers support bioreactor-expanded VM ReN cells as neural progenitors

Maintaining NPCs in an undifferentiated state in bioreactors is crucial for ensuring a stable source of therapeutic

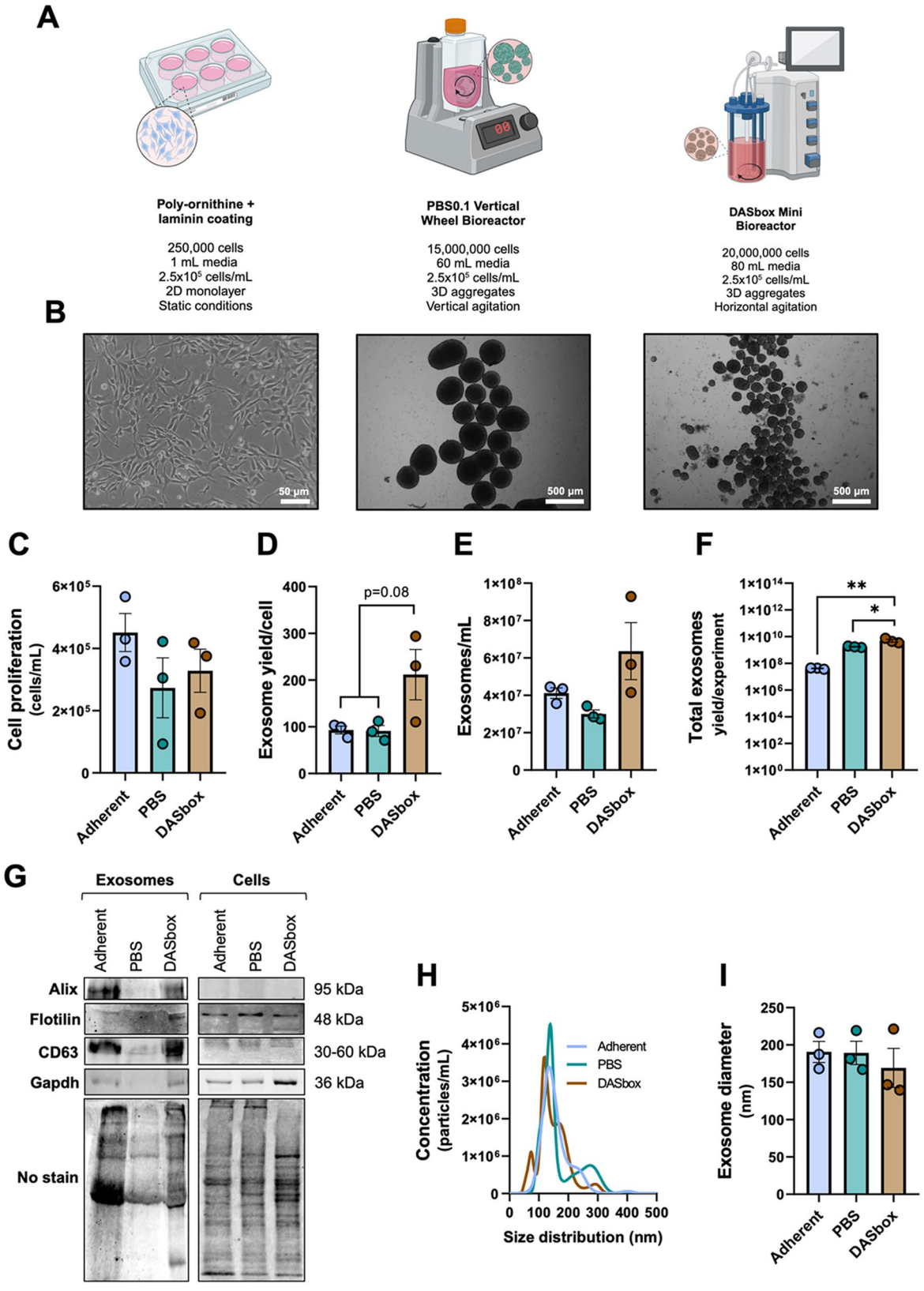

Fig. 1 (See legend on next page.)

(See figure on previous page.)

Fig. 1 Bioreactors increase ReN cell yield and exosome production compared to 2D adherent cultures. (**A**) Schematic representation of ReN cell seeding (250,000 cells/mL) in 2D adherent cultures and 3D bioreactors (PBS Mini 0.1 and DASbox Mini). (**B**) Representative brightfield images of cells and neurospheres at 48 h, in each condition. (**C**) Cell proliferation after 48 h in culture (cells/mL), shows no significant differences between 2D static or 3D bioreactor systems ($p = 0.317$). (**D**) Production of exosomes from DASbox-upscaled ReN cells, normalized per cell (secretory efficiency) are slightly increased compared with the other conditions ($p = 0.08$). (**E**) Exosome concentration in conditioned media, expressed as exosomes/mL, tends to be enhanced in the DASbox condition (differences between groups: $p = 0.095$). (**F**) Cumulative exosomal yield, calculated as exosomes/mL × total culture volume (mL), shows significant differences between groups ($p = 0.006$), being significantly increased in bioreactors. **(G)** Western blot analysis of exosomal protein markers confirms exosome identity and purity. A total of 20 µg of protein of each condition was loaded per sample. Exosome samples show enrichment of canonical exosomal markers Alix and CD63 when compared to producer cell lysates. (**H**) Size distribution profiles of exosomes derived from adherent and bioreactor system cell cultures by Nanoparticle Tracking Analysis show similar profiles and peak diameters across conditions. (**I**) Mean exosome diameters are consistent across all culture systems ($p = 0.694$). Data are mean ± SEM, from three independent experiments. Statistical differences were assessed by one-way ANOVA, followed by post-hoc Tukey comparisons. $^{*}p < 0.05$ and $^{**}p < 0.01$

exosomes. Undifferentiated cells produce exosomes rich in growth factors and signaling molecules essential for neuronal health [13, 49]. Moreover, preserving this status reduces variability in cell behavior and exosome composition, essential for standardizing bioprocessing methods and ensuring therapeutic efficacy. To investigate whether human ReN cells maintained their undifferentiated phenotype during the 6 days of expansion in bioreactors, we assessed neural progenitor and neuronal differentiation markers by Western blot, comparing them to undifferentiated and differentiated ReN cells (Fig. 3A).

Various markers have been used to assess pluripotency and neural differentiation. We analyzed the expression of the stemness markers nestin and Sox2 alongside the neuronal markers β-III-tubulin and tau in the ReN cells under different culture conditions. Sox2, a key transcription factor for neural progenitor identity and self-renewal capacity [50, 51] (in green, Fig. 3B, C), decreased from undifferentiated to differentiated cells, though not significantly, with a small reduction in DASbox cells compared to PBS cells, thus mostly preserving the stemness levels of undifferentiated cells (Fig. 3C).

Nestin, an NPC marker upregulated at the onset of neural differentiation [52] (early neural processes, in pink color, Fig. 3B), remained mostly consistent, with a slight, non-significant increase in bioreactor systems, particularly in the PBS (Fig. 3D). Neuronal markers, β-III-tubulin, expressed during the late phase of neural differentiation and maintained high in mature neuronal cell types [53], as well as tau that correlates with neural maturation [54], increased significantly in differentiated ReN cells, with levels in bioreactor-grown aggregates similar to undifferentiated cells (dark pink, Fig. 3B, E-F).

To further explore the interplay between stemness and differentiation, we calculated the ratios between the corresponding markers. The Sox2/β-III-tubulin ratio revealed significant differences between undifferentiated cells and those cultured in bioreactors, suggesting a decrease in self-renewal capability, but still higher than in fully differentiated cells (Fig. 3G). The nestin/β-III-tubulin ratio showed a significant difference between undifferentiated and differentiated cells, indicating a predominance of NPCs in both bioreactor systems (Fig. 3H). In contrast, the tau/Sox2 and tau/nestin ratios displayed an opposite trend, in that they were similar between undifferentiated and bioreactor-cultured cells, but significantly different from differentiated cells (Fig. 3I, J), thus confirming the predominance of NPCs.

Unsupervised hierarchical clustering of the ReN cell samples, based on their stemness and neuronal marker expression, grouped undifferentiated, PBS and DASbox cells together, indicating that the expression profiles of undifferentiated cells are more similar to those in the bioreactor conditions than to those in differentiated cells, which form a separate cluster (Fig. 3K). These results suggest that both bioreactor systems maintain a substantial NPC population.

Differentiated cells and bioreactor-expanded ReN cells originate exosomes that are slightly enriched in miRNAs

In previous studies, we assessed a set of inflammatory-associated miRNAs (miR-124, miR-146a, miR-155, miR-21b and miR-125b) commonly identified in glial and neuronal cells, as well as in their derived exosomes, which we found to be dysregulated during neurodegeneration and inflammation [37, 38, 48, 55]. miRNAs, noncoding RNAs that regulate gene expression post-transcriptionally, are part of the exosomal cargo [56] and can be then transferred from donor cells to recipient cells in this way [57].

Considering our goal of using ReN-derived exosomes loaded with miRNA mimics and inhibitors for the treatment of neurodegenerative diseases, we assessed the expression of this set of miRNAs. Our interest is driven by recent findings reporting that bioreactor-based upscaling of exosome production may alter miRNA cargo [24], as well as their regulation by biophysical forces, such as the upregulation of miR-21 under shear stress [58, 59]. In addition, the miRNA content of exosomes may vary depending on the cell source [60, 61], and we hypothesize that differentiation state also plays a role.

Therefore, we investigated three key questions: (i) whether the miRNA profile of exosomes derived from SH-*WT* neuroblastoma cells, used in some of our

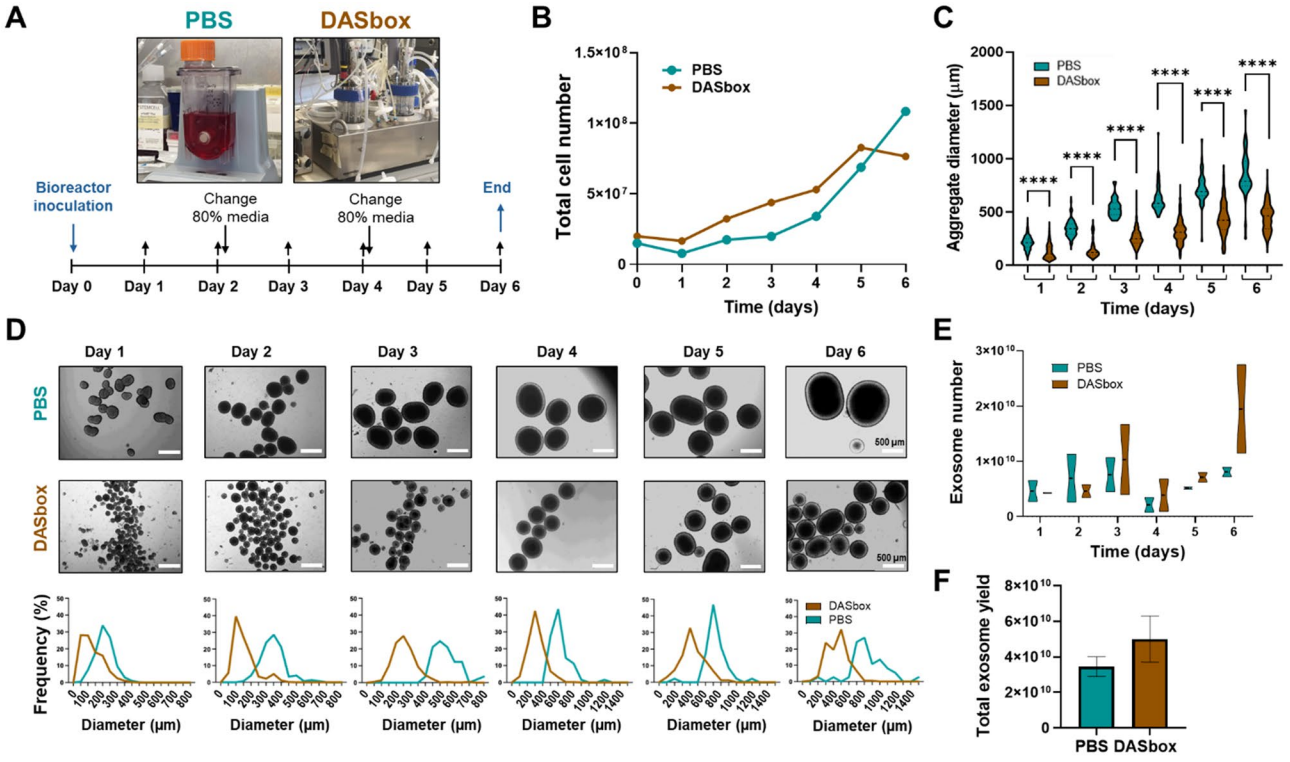

Fig. 2 NPCs expansion in DASbox bioreactors results in smaller neurospheres and greater exosome production than PBS systems. Three independent bioreactor assays per condition were run until day 6. (**A**) Experimental setup: bioreactors were inoculated with 2.5×10^5 cells/mL on day 0; sampling, including aggregate quantification and conditioned media collection, was performed daily (↑), and every 2 days, 80% of the culture medium was replaced (↓). (**B**) Cell proliferation over 6 days of culture, showing growth kinetics in PBS and DASbox systems. Cell concentration (cells/mL) was measured daily from day 1 to day 6 to assess proliferation dynamics. (**C**) Aggregate size dynamics of ReN cells, in terms of average aggregate diameter per day (bioreactor type, $p = 0.04$; day, $p < 0.0001$; bioreactor x day, $p = 0.02$). (**D**) Representative neurosphere images and size distribution histograms. (**E**) Daily exosome concentration (exosomes/mL) in each bioreactor system (bioreactor type, $p = 0.41$; day, $p = 0.09$; bioreactor type x day, $p = 0.48$). (**F**) Cumulative exosome yield collected from PBS and DASbox bioreactors at the end of the 6-day culture period (*$p = 0.38$*). Statistical differences were evaluated by two-way ANOVA followed by post-hoc Tukey's comparisons (multiple groups) or *t*-test (two groups). ****$p < 0.0001$

previous studies, differs from those of ReN cells; (ii) how neuronal differentiation status may affect miRNA content in each cell type's exosomes; and (iii) whether exosomes from bioreactor-expanded ReN cells differ from those from static cultures.

No significant differences were observed between SH-*WT* and ReN-derived exosomes, whether from undifferentiated or differentiated cells, in their miRNA cargo, suggesting similar levels across both cell lines (Fig. 4A-E). However, ReN-derived exosomes had slightly lower miR-21-5p content than SH-*WT*-derived exosomes (*$p = 0.08$*, Fig. 4D). When comparing within the SH-WT cell line, exosomes from undifferentiated cells showed higher miR-124-3p and miR-21-5p levels than those from differentiated cells (*$p < 0.05$*, Fig. 4A), with a similar trend observed for miR-146a-5p (*$p = 0.09$*, Fig. 4D).

To further assess if miRNA distribution from cells into exosomes was similar when dealing with undifferentiated or differentiated cells, we calculated the exosomal-to-cellular miRNA ratio in a pool sample (Fig. 4F). These preliminary data, while limited, are interesting to show that miRNA content was approximately 10^3 fold higher in exosomes than in the cells of origin when differentiated, as well as in expanded ReN cells in the DASbox bioreactor, mainly for miR-124-3p, miR-146a-5p and miR-155-5p, suggesting active transport from cells to exosomes, probably as waste products. In contrast, the exosomal-to-cellular miRNA ratio was closer to 1 or lower in undifferentiated cells, suggesting passive transport or intracellular retention, possibly due to cell requirements. Further studies with larger sample numbers are needed to confirm these results.

Next, we determined whether ReN cell-derived exosomal miRNA expression levels differ between the static cultures and those under shear stress in bioreactors. We noticed that both bioreactor systems tend to enhance the exosomal miRNA levels as compared to adherent cells (Fig. 4G-K). Indeed, exosomes from PBS and DASbox-expanded ReN cells showed trends toward higher levels of miR-124-3p (*$p < 0.10$*, Fig. 4G). In the same way, we observed a similar trend only for miR-146a-5p and miR-125b-5p in exosomes derived from the DASbox

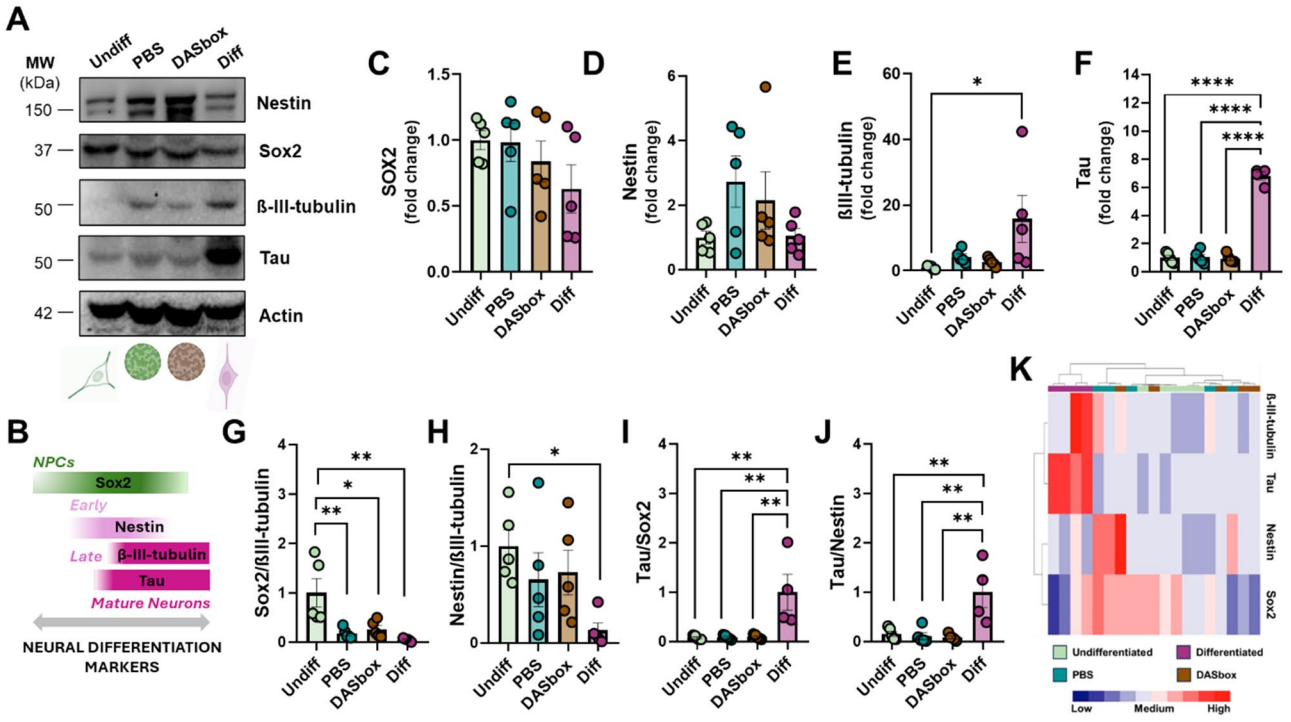

Fig. 3 ReN cells expanded in bioreactors for 6 days predominantly express undifferentiated neural progenitor markers. (**A**) Representative Western blot images for stemness and neuronal biomarkers in ReN cells grown in 2D in monolayers and 3D aggregates grown in PBS and DASbox bioreactors. (**B**) Change in the expression of neural markers through the differentiation of neural progenitor cells into early and late mature neurons. (**C**) Sox2 protein expression analysis ($p = 0.28$). (**D**) Nestin protein expression analysis ($p = 0.17$). (**E**) ß-III-tubulin expression analysis ($p = 0.045$). (**F**) Tau expression analysis ($p < 0.0001$). (**G**) Sox2/ß-III-tubulin undifferentiation rate ($p = 0.0017$). (**H**) Nestin/ß-III-tubulin undifferentiation rate ($p = 0.052$). (**I**) Tau/Sox2 differentiation rate ($p = 0.002$). (**J**) Tau/nestin differentiation rate ($p = 0.001$). (**K**) Unsupervised hierarchical clustering of ReN cells based on their expression of stemness and differentiation markers. Data were row-standardized to facilitate comparisons across conditions. Clustering used Pearson correlation (rows), Euclidean distance (columns) and the Ward's linkage method. Data are mean ± SEM from five experiments. Statistical differences were assessed by one-way ANOVA, followed by post-hoc Tukey's comparisons. *$p < 0.05$, **$p < 0.01$, ***$p < 0.001$ and ****$p < 0.0001$ Sox2, SRY-Box transcription factor 2

bioreactor cultures ($p < 0.10$, Fig. 4H, K). These results suggest that exosomes from bioreactor-expanded ReN cells are enriched in miRNAs when compared with the respective adherent cultures, potentially enhancing their efficiency to target the recipient cells.

Loading of miR-124-3p mimic in ReN-derived exosomes and delivery into microglia is improved in the DASbox bioreactor-expanded ReN cell condition

We and others have previously shown that miR-124-3p has neuroprotective properties in Parkinson's disease and AD models [26, 31], promotes neurogenesis after ischemia [62], attenuates neuroinflammation and promotes neuronal repair and plasticity after traumatic brain injury [63]. Exosomes enriched with miR-124-3p have already been used in therapies for diseases like Huntington's [64] and Parkinson's [31], as well as repetitive mild traumatic brain injury [65]. However, none of these studies used human NPC-derived exosomes or applied bioreactor-based upscaling before using the Exo-Fect™ Exosome Transfection Kit. Here, we started by comparing the transfection efficiency of pre-miR-124-3p in exosomes from 2D adherent cultures and bioreactor scale-up (PBS and DASbox) to explore their potential for AD cell-free therapies (Fig. 5A).

Compared with mock-transfected controls (without miR-124-3p mimic), all transfected exosomes showed a significant increase in miR-124-3p cargo ($p < 0.0001$), regardless of culture conditions (Fig. 5B). Notably, exosomes isolated from DASbox-expanded ReN cells exhibited a higher transfection efficiency than those from PBS bioreactors ($p < 0.01$).

Subsequently, we investigated the uptake of pre-miR-124-3p transfected exosomes from the three culture conditions by CHME3 microglia, professional brain phagocytes [66]. Microglial cells successfully internalized exosomes from all source conditions without showing any gross morphological alterations (Fig. 5C). Quantification showed a mild elevation in the uptake of DASbox-upscaled exosomes compared to those from adherent or PBS cultures (Fig. 5D). No differences in PKH26 labeling intensity were observed across exosome sources, ruling out preferential labeling of some exosomes over others (Fig. 5E). Although no statistical differences were found,

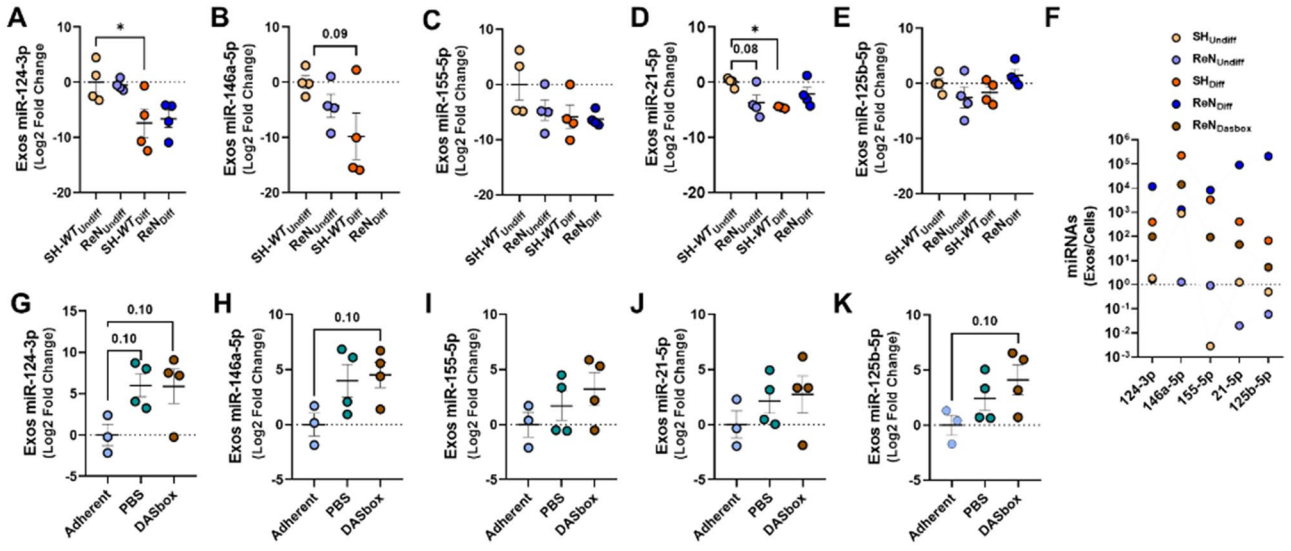

Fig. 4 ReN-derived exosomes display miRNA profiles similar to SH-*WT* cells and mild miRNA enrichment post-bioreactor expansion. (**A-E**) Analysis of exosomal miRNA expression profile in different cell lines and differentiation status. (**A**) miR-124-3p: cell line, $p = 0.94$; status, $p = 0.0027$; cell line x status, $p = 0.72$. (**B**) miR-146a-5p: cell line, $p < 0.0001$; status, $p < 0.0001$; cell line x status, $p < 0.0001$. miR-146a-5p levels were below detection levels in ReN cell differentiated samples. (**C**) miR-155-5p: cell line, $p = 0.23$; status, $p = 0.09$; cell line x status, $p = 0.31$. (**D**) miR-21: cell line, $p = 0.54$; status, $p = 0.16$; cell line x status, $p = 0.01$. (**E**) miR-125b-5p: cell line, $p = 0.84$; status, $p = 0.37$; cell line x status, $p = 0.04$. **(F)** Exosomal-to-cellular miRNA ratio profiles in a pooled sample ($n = 4$ samples/condition). (**G-K**) Analysis of exosomal miRNA profile under different culture conditions. (**G**) miR-124-3p ($p = 0.07$). (**H**) miR-146a-5p ($p = 0.08$). (**I**) miR-155-5p ($p = 0.32$). (**J**) miR-21-5p ($p = 0.43$). (**K**) miR-125b-5p ($p = 0.11$). Data are mean ± SEM from three-to-four independent samples. Statistical differences were assessed by two-way ANOVA (considering cell line and differentiation status as factors), followed by post-hoc Tukey's comparisons. *$p < 0.05$. Exos, exosomes

DASbox-upscaled exosomes showed slightly higher microglia internalization, suggesting potential benefits for therapeutic applications.

To test our hypothesis that DASbox-upscaled exosomes are internalized more efficiently by the microglia, we investigated the cell impact of pre-miR-124-3p transfected exosomes. Pre-miR-124-3p transfected exosomes from all sources significantly increased intracellular miR-124-3p levels, with DASbox-upscaled exosomes being the most effective (Fig. 5F). We can further estimate the exosome uptake efficiency, expressed as the proportion of exosomes initially applied, as follows: 3.82 ± 0.23% for adherent, 7.09 ± 1.51% for PBS and 9.32 ± 1.94% for DASbox exosomes. These calculations should be considered approximate values, as they are based on theoretical estimates of both the input and the number of recipient cells. This suggests that improved internalization may enhance the therapeutic effect of DASbox-upscaled exosomes. However, a more precise assessment of uptake efficiency could be achieved in future studies by directly quantifying the number of exosomes remaining in the supernatant before and after incubation (e.g., by NTA or tunable resistive pulse sensing).

DASbox-scalable exosomes enriched with miR-124-3p mimic are captured by neuron-glia cells and protect from cellular stress and inflammation

Several recent reports support exosomes as important mediators of neuron-astrocyte-microglia cell communication [67, 68] and their promising outcomes in preclinical contexts. Exosomes enhance neuronal vitality, reduce neuroinflammation and promote synaptic dynamics [69]. Moreover, the engineering of exosomes with selected miRNAs was shown to amplify their therapeutic efficacy in neurodegenerative diseases and brain injury [70, 71]. However, their production is complex and time-consuming, influenced by cell culture conditions and source-target cell interactions. After DASbox-scalable exosomes demonstrated the best functional properties under the tested conditions, we then assessed basal miR-124 levels in neuronal and glial cells before loading them with miR-124 mimic.

Neuronal-like cells included SH-*WT* and SH-*SWE* (the latter mimicking AD), while glial cells included immortalized primary human cortical astrocytes (IM-HA) and immortalized human microglia (CHME3) cell lines. As expected, SH-*WT* and SH-*SWE* neuroblastoma cells exhibited higher miR-124-3p levels than astrocytes (not significant) and microglia ($p < 0.05$, Fig. 6A), aligning with the preferential location of miR-124-3p in neurons, their derived exosomes, and its role in neurogenesis and neuroprotection.

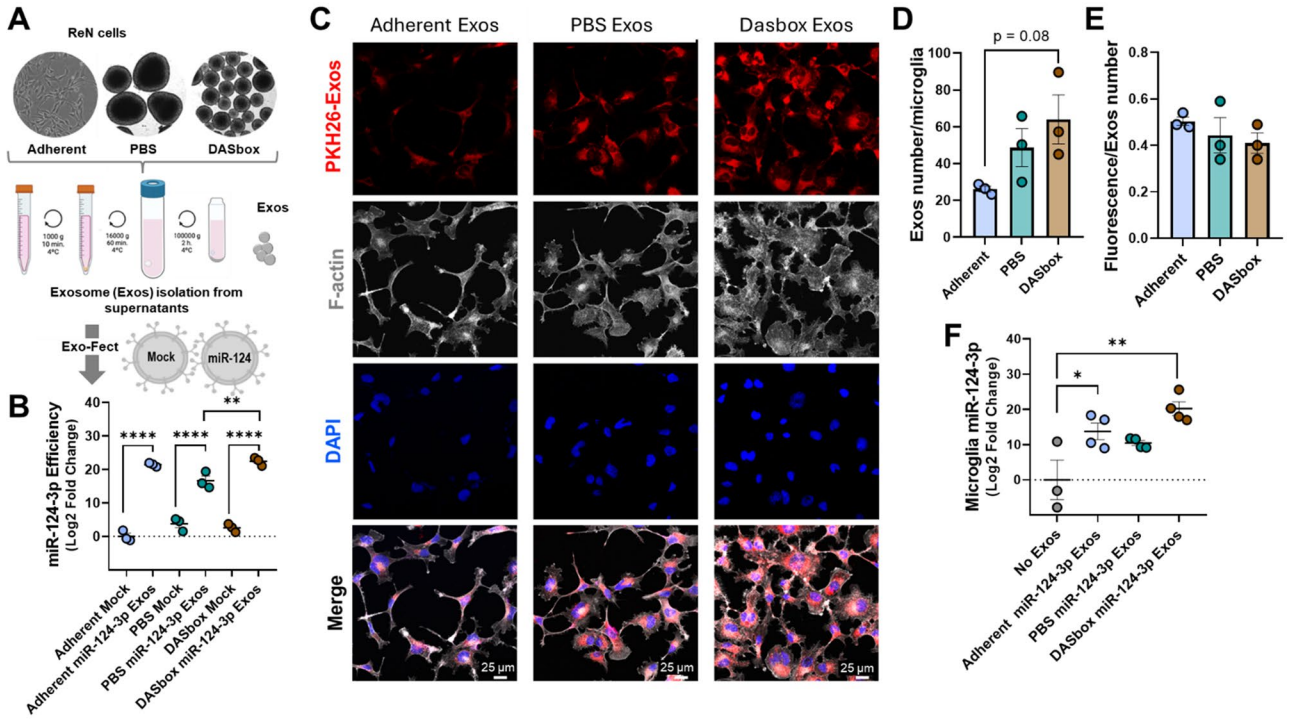

Fig. 5 ReN cell-derived exosomes (Exos) are efficiently transfected with pre-miR-124-3p, with DASbox-derived Exos enhancing microglial miR-124-3p enrichment. (**A**) Schematic representation of ReN cell cultures in adherent (2D) and in PBS/DASbox bioreactor 3D conditions, followed by supernatant ultracentrifugation and transfection. (**B**) ExoFect transfection efficiency of Exos from each condition, using pre-miR-124-3p ($p = 0.003$). (**C**) Representative images of Exos internalization by CHME3 microglia immunostained for F-actin (grey), after incubation with PKH26-labelled Exos (red) and nuclear visualization with DAPI (blue). (**D**) Internalized DASbox-derived Exos per microglial cell are mildly elevated as compared with the adherent-produced Exos ($p = 0.086$). (**E**) PKH26 fluorescence intensity shows similar labeling for all the ReN-Exos source conditions ($p = 0.47$). (**F**) miR-124-3p expression levels are increased in microglia treated with adherent- and DASbox-derived ReN Exos transfected with pre-miR-124-3p (miR-124 Exos; $p = 0.003$). Data are mean ± SEM from 3–4 independent experiments. Statistical differences were assessed by one-way ANOVA followed by Tukey's post-hoc tests. $^{*}p < 0.05$, $^{**}p < 0.01$ and $^{****}p < 0.0001$

To evaluate the potential of exosomes to target multiple CNS cell types, we investigated whether neurons and astrocytes—unlike microglia, which are inherently phagocytic—were also capable of internalizing these DAS-box-derived exosomes from upscaled ReN cells (naïve ReN-exosomes). To this end, we exposed neurons and glial cells to PKH26-labeled naïve ReN-exosomes for 24 h and analyzed their cellular uptake using confocal microscopy (Fig. 6B). Exosomes were readily internalized by all cell types, as evidenced by the widespread distribution of red fluorescence dots throughout the cytoplasm, frequently concentrated in perinuclear regions. These findings demonstrate that not only microglial cells but also neurons and astrocytes efficiently internalize exosomes, supporting their use as versatile delivery vehicles across diverse brain cell populations.

Once our future goal is to use DASbox-upscaled naïve ReN-exosomes transfected with pre-miR-124-3p (DASbox miR-124-3p Exos) to prevent/halt/repair neurodegeneration and neuroinflammation, we decided to evaluate cell miR-124-3p level alterations after their interaction with cells and determine a parameter that could reflect the initial and final cell neuroinflammation-associated state. To this end, we induced neural aging dysfunction using mild concentrations of H_2O_2 in both SH-*WT* and the SH-*SWE* cells [72]. SH-*SWE* cells were used as a common pathological AD model [27] and effects were compared to those of SH-*WT* cells in the same conditions. In the case of glial cells we stimulated astrocytes with IL-1α + TNF-α + C1q [73], and microglia with IFN-γ + H_2O_2 to mimic late-stage AD [74], comparing outcomes to non-stimulated matched cells.

H_2O_2 treatment in SH-*WT* cells reduced miR-124-3p levels ($p = 0.063$), while naïve ReN-exosomes significantly increased its levels, probably due to their natural increased miR-124-3p content (Fig. 6C). Intriguingly, miR-124-3p exosomes did not further elevate miR-124-3p levels either in H_2O_2 untreated or treated cells, suggesting that these cells may quickly use or even release this miR-124 in newly formed exosomes. However, in the presence of H_2O_2 treatment, the addition of naïve ReN-exosomes caused a significant increase of miR-124-3p level in SH-*WT* cells, as compared with cells not treated with exosomes ($p < 0.05$). We then decided to assess the

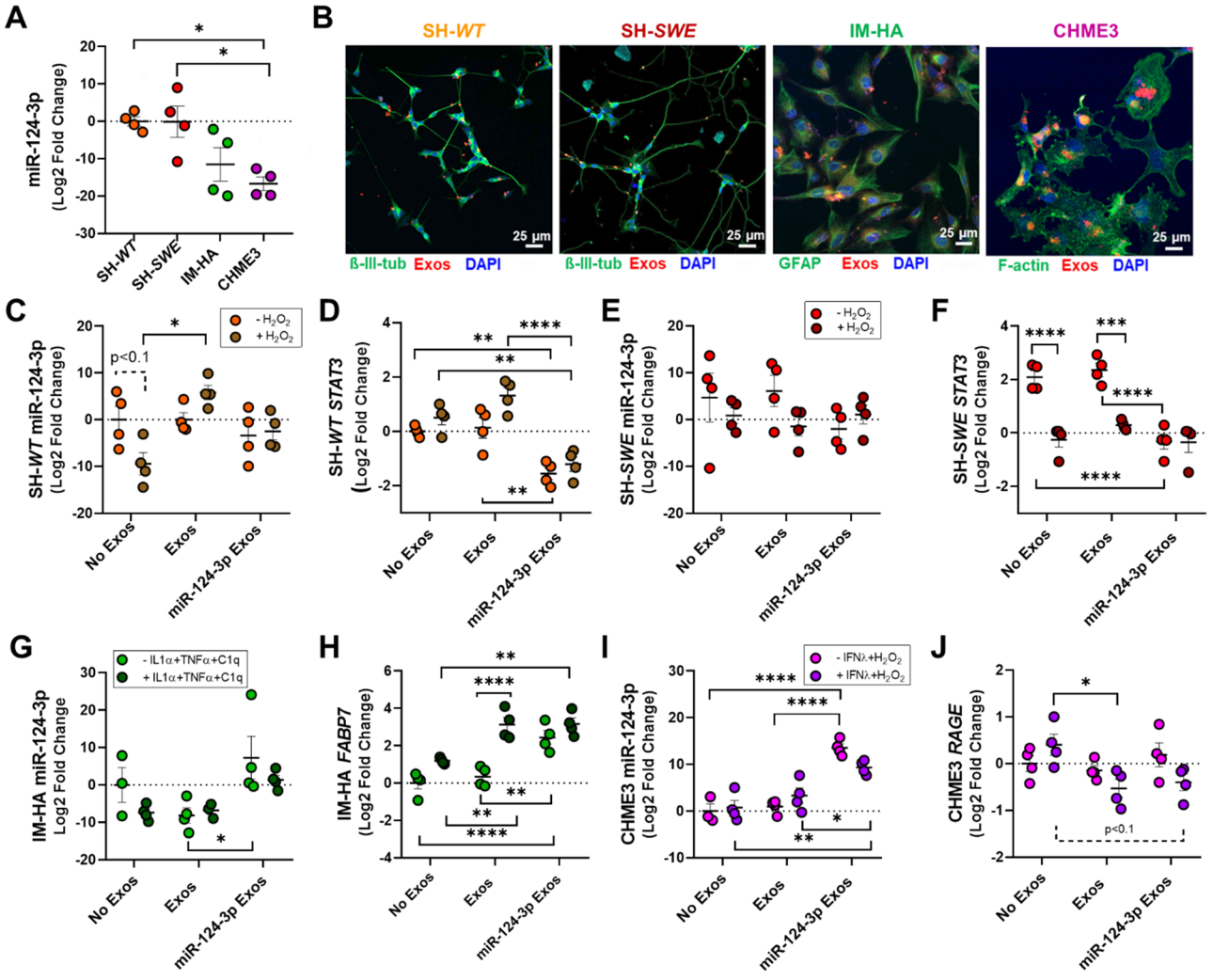

Fig. 6 Neurons and glia internalize miR-124-3p-loaded ReN-exosomes, enhancing cell-type-specific modulation of inflammation-related genes compared with naïve exosomes. (**A**) Endogenous miR-124-3p levels in SH-*WT* and SH-*SWE* neurons, IM-HA astrocytes, and CHME3 microglia differ significantly ($p = 0.007$). (**B**) PKH26-labeled naïve ReN-exosomes (red) in neuronal (β-III-tubulin, green), astrocytic (GFAP, green), and microglial (F-actin, green) cells; nuclei were stained with DAPI (blue). (**C**) miR-124-3p levels in SH-*WT* cells in tested conditions (H_2O_2, $p = 0.006$; exosomes, $p < 0.0001$; H_2O_2 X exosomes, $p = 0.009$). (**D**) *STAT3* gene expression in SH-*WT* cells in tested conditions (H_2O_2, $p = 0.62$; exosomes, $p = 0.008$; H_2O_2 X exosomes, $p = 0.009$). (**E**) miR-124-3p levels in SH-*SWE* cells in tested conditions (H_2O_2, $p = 0.27$; exosomes, $p = 0.51$; H_2O_2 X exosomes, $p = 0.22$). (**F**) Expression of *STAT3* in SH-*SWE* cells in tested conditions (H_2O_2, $p < 0.0001$; exosomes, $p < 0.0001$; H_2O_2 X exosomes, $p = 0.006$). (**G**) miR-124-3p levels in IM-HA cells in tested conditions (IL1α/TNFα/C1q treatment, $p = 0.154$; exosomes, $p = 0.006$; interaction, $p = 0.392$). (**H**) Expression of *FABP7* in IM-HA cells in tested conditions (IL1α/TNFα/C1q treatment, $p < 0.0001$; exosomes, $p < 0.0001$; interaction, $p = 0.009$). (**I**) miR-124-3p levels in CHME3 cells in tested conditions (IFNγ + H_2O_2 treatment, $p = 0.711$; exosomes, $p < 0.0001$; interaction, $p = 0.036$). (**J**) Expression of *RAGE* in CHME3 cells in tested conditions (IFNγ + H_2O_2 treatment, $p = 0.24$; exosomes, $p = 0.038$; interaction, $p = 0.044$). Human differentiated SH-SY5Y (SH-*WT*) and SH-Swedish (SH-*SWE*) neuroblastoma cells were either unstimulated (-H_2O_2) or stimulated (+H_2O_2) before treatment with naïve ReN-exosomes (Exos) or DASbox miR-124-3p Exos. Immortalized human astrocytes (IM-HA) were either unstimulated (-IL1α/TNFα/C1q) or stimulated (+IL1α/TNFα/C1q) before treatment with naïve ReN-exosomes (Exos) or DASbox miR-124-3p Exos. CHME3 human microglial cells were either unstimulated (-IFNγ + H_2O_2) or stimulated (+IFNγ + H_2O_2) before treatment with naïve ReN-exosomes (Exos) or DASbox miR-124-3p Exos. Data represent mean ± SEM from 4 independent experiments. Statistical differences were assessed by multi-way ANOVA followed by Tukey post-hoc tests; only biologically relevant differences are shown. *STAT3*, gene that encodes the signal transducer and activator of transcription 3; *FABP7*, fatty acid binding protein 7; *RAGE*, receptor for advanced glycation end products: Exos, exosomes; miR, microRNA

effects caused by naïve and transfected exosomes in the SH-*WT* cell homeostasis by determining the expression levels of *STAT3*, indicated as promoting neuroinflammation [75]. Notably, miR-124-3p exosomes significantly decreased *STAT3* in SH-*WT* cells, regardless of H_2O_2 treatment, when compared with cells that did not receive exosomes or were treated with the naïve ones (at least $p < 0.01$, for all the conditions, Fig. 6D), attesting their beneficial effect.

No alterations were noticed in the SH-*SWE* cells in terms of miR-124-3p levels (Fig. 6E). Like SH-*WT* cells, miR-124 exosomes significantly decreased *STAT3*

compared to naïve exosomes or in their absence, without H_2O_2 treatment (Fig. 6F). Notably, the ageing effect by the mild concentration of H_2O_2 resulted in a significant reduction of *STAT3* only in the pathological SH-*SWE* cells without or with naïve exosomes (at least $p < 0.001$) (Fig. 6F), highlighting the increased sensitivity of SH-*SWE* cells to *STAT3* reduction by H_2O_2 and to the effective miR-124 exosomes targeting, thus suggesting protection against neuroinflammation and neuronal death. Further studies should investigate additional defensive processes by miR-124-3p-loaded exosomes, their recognition by the neuroblastoma cells and if exosomal fusion with cell membrane is implicated.

In astrocytes, as expected, the stressful cocktail caused a mild miR-124 reduction, which was maintained by the addition of exosomes (Fig. 6G), suggesting a reactive phenotype. However, miR-124-3p engineered exosomes significantly upregulated miR-124-3p levels, mainly in the naïve condition ($p < 0.05$). To assess potential effects on astrocyte reactivity, we analyzed *FABP7* expression, a gene that encodes the fatty acid binding protein 7, indicated as protecting from the induction of inflammation [76]. Exosome exposure, particularly miR-124-3p-loaded exosomes, significantly increased *FABP7* expression under inflammatory conditions ($p < 0.01$, Fig. 6H), thus suggesting a role for miR-124-3p in regulating astrocytes reactivity, though requiring future more detailed studies.

Microglial cells, as professional phagocytes, exhibited the strongest response to miR-124-3p exosomes (Fig. 6I). Both unstimulated and IFNγ + H_2O_2 stimulated microglia showed significantly increased intracellular miR-124-3p levels following miR-124-3p exosome incubation compared to naïve and exosome-treated cells (Fig. 6I). We determined the microglial marker *RAGE* that encodes for the receptor for advanced glycation end products and is related with increased susceptibility to neurodegeneration and neuroinflammation [77, 78]. Naïve exosomes significantly decreased *RAGE* expression, while miR-124 exosomes showed a tendency ($p = 0.08$) in microglia under stressful conditions (Fig. 6J), supporting the benefits of both naïve and miR-124-enriched exosomes.

Our findings demonstrate that neurons, astrocytes, and microglia can internalize neural exosomes but respond differently to miR-124-3p modulation. Microglia showed the greatest sensitivity to exosome treatment, followed by neurons, while astrocyte responses were more context-dependent. In summary, DASbox-upscaled exosomes and their loading with miR-124-3p hold promise for mitigating neurodegeneration, neuroimmune dysregulation and glial activation in ageing-associated neurodegenerative diseases, such as AD.

Discussion

Exosome-based drug delivery is a promising field with the potential to transform therapeutic approaches. Exosomes transfer functional proteins, metabolites and nucleic acids into recipient cells [79]. Varied contents of exosomes have been shown to aid regeneration, from growth factors such as vascular endothelial growth factor to miRNAs [80]. Moreover, unlike conventional drug delivery systems, exosomes offer unique advantages such as excellent biocompatibility, low immunogenicity, and reduced toxicity. Therefore, they can be engineered for targeted delivery and improved stability, making them valuable for regenerative medicine [81]. Nonetheless, integrating exosomes into clinical practice faces several challenges, including low exosomal yield, often insufficient for clinical applications [82], costly isolation methods, and scalability issues [16]. Addressing these challenges requires a scalable production method, able to generate a clinically relevant number of exosomes, but also ensuring consistent exosome properties. A recent study has shown that the upscaling of exosomes secretion from MSCs relative to adherent cells increases the yield by 2.4-fold [83]. Actually, traditional 2D cultures limit exosome yield due to restricted cell growth, limited by the surface area of the culture plastic, whereas 3D bioreactors provide a physiologically favorable environment that enhances cell interactions and exosome secretion [16]. Using the PBS Mini 0.1 L vertical-wheel bioreactor system, Jeske et al. observed that the bioreactor system promoted exosome secretion from human MSCs by 2.5-fold and upregulated biogenesis markers, glycolysis genes and miRNA cargo compared to the static 2D culture [24]. Lately, a smaller scale, the miniaturized version for small-scale stem cell culture experiments, the DASbox, was described by Ulpiano et al. [84].

Exosomes like stem cells provide clinical benefits but do not have the biosafety concerns of the living cell transplantation [85]. For instance, both MSC- and NSC-derived exosomes have shown neuroprotective properties in AD [86]. In contrast to other cell-type-derived exosomes, these stem-derived vesicles possess antioxidant, anti-apoptotic and immunomodulatory properties [87]. With respect to NSC/NPC-derived exosomes, they inherit neuroprotective and neuroregenerative potential and immunomodulatory capabilities from the parent cells and participate in intercellular communication [6]. Nevertheless, while NSC-exosomes facilitate NSC differentiation [15], NPC-derived exosomes demonstrated to suppress microglial activation and to protect neurons from apoptosis [88].

Based on these assumptions and our objectives to apply the upscaled exosomes for their neuroprotective and neuro-immune reparative properties we here used ReN

cells as NPCs to compare their exosome production by PBS, DASbox, and adherent monocultures.

Our findings confirm that bioreactors, particularly the DASbox Mini system, significantly increase exosomal yield compared to 2D methods, aligning with previous studies on 3D culture advantages [89, 90]. Indeed, this bioreactor produced 1.5 times more exosomes per mL than PBS system or 2D cultures, a difference not statistically significant but biologically relevant. Importantly, ReN cells exhibited comparable proliferation rates across conditions, with similar cell densities after 48 h, despite a slight delay in doubling time observed in the PBS bioreactor. This suggests that the increase in exosome output is not merely due to higher cell numbers but likely reflects improved functional performance under dynamic 3D culture conditions. Our results are consistent with previous reports showing enhanced EV production in high-density culture systems. For instance, the CELLine 1000-AD model, while supporting high-density growth similar to a bioreactor, does not provide precise environmental control; nevertheless, it has been reported to increase EV yield compared to conventional 2D cultures [91]. This highlights that dynamic and controlled 3D culture systems, such as the DASbox Mini bioreactor used here, may further optimize exosome production beyond what is achievable in static high-density flasks.

Bioreactors provide physiologically relevant 3D environment that supports natural cell growth, enhancing cell-to-cell interactions and dynamic behavior [92]. These conditions are crucial for exosome secretion, as they better mimic the signals that regulate vesicle release [16] and may underlie the improved exosome yield observed in the present study. Our better results with the DASbox bioreactor can be related with its ability to optimize culture conditions by regulating nutrient availability, oxygen levels, and waste removal. Indeed, this bioreactor maintains a stable environment with controlled temperature and pH, promoting faster cell proliferation and higher exosome yields [84, 93]. Interestingly, we observed a trend toward higher exosome secretion per cell in the DASbox condition, suggesting that this system may enhance the intrinsic secretory capacity of individual cells, not just the volumetric yield [89, 94]. This is particularly relevant when aiming to maximize production efficiency without necessarily expanding cell numbers. Furthermore, the absolute exosome yield in the DASbox bioreactor was over 100-fold higher than that obtained in the adherent culture, underscoring the biotechnological potential of this system for scalable exosome production. Our study demonstrates the feasibility of scalable hNPC-derived exosome production in the two bioreactor systems; however, we acknowledge that aggregate size and exosome yield are likely influenced by hydrodynamic differences and other bioreactor parameters, such as oxygen tension, pH, and feeding regime, which were not systematically optimized in this work and represent important directions for future investigation.

After confirming that ReN cells in bioreactors produce significantly more exosomes than in 2D cultures, we scaled up exosome production in each bioreactor system to further enhance exosome yield. The DASbox bioreactor consistently produced smaller neurospheres than the PBS device, likely due to improved nutrient access. As neurospheres grow, outer-layer cells remain well-nourished, while central cells risk deprivation, creating a nutrient gradient [18]. Despite this, daily sampling showed minimal trypan blue-positive dead cells in both systems, indicating high viability. However, prolonged culture may require dissociation or increased agitation to maintain cell viability and pluripotency.

One of the concerns of using bioreactors to enhance exosome production relates with hypothetical changes in exosomal size that may derive from the bioreactor system, cell type and culture conditions, with effects on biological activity and therapeutic applications [95]. Exosome diameter distribution, assessed as recommended in MISEV2023 guidelines [1] highlighted that the main exosomal size remained consistent between 2D and 3D cultures, with average diameters of 170–190 nm, and a smaller subset of larger vesicles. While exosomes are typically 30–150 nm in diameter, the larger sizes observed may result from the approach used to quantify particle size, NTA, which relies on the mobility of particles and tends to overestimate particle diameter compared to other methods such as cryo-electron microscopy [96], though it can also derive from vesicle aggregation [24]. The consistency in size across culture conditions in our study suggests that exosome formation mechanisms remain stable, regardless of the transition from 2D to bioreactor settings. Also, the exosome protein markers used for their characterization [1], such as Alix (with lipid or membrane protein-binding ability) and CD63 (a multipass transmembrane protein), were particularly evident in those derived from Adherent and DASbox cultures.

Exosomes have been pursued recently as a cell-free alternative to stem cell-based therapy. Embryonic and induced pluripotent stem cells, as well as the multipotent stem cells, such as hematopoietic, mesenchymal, neuroprogenitor and endothelial-derived exosomes became important due to the pluripotency or multipotency of their parental cells [14]. So, one crucial factor to consider when evaluating NPC-derived exosomes for clinical applications is the differentiation status of the producing cells. In our study, bioreactor-cultured neurospheres expressed nestin and Sox2 at levels like undifferentiated ReN cells, retaining multipotentiality, consistent with findings from large-scale stirred-tank bioreactor cultures of mouse NPCs [97].

As exosomes carry miRNAs and may be enriched with them for therapeutic applications [70, 98], including for targeting neuroinflammation where miR-155 and miR-146a have a critical role [99], we assessed five selected inflammatory miRNAs in exosomes from ReN cells under different culture conditions, which have been shown to regulate neuro-immune homeostasis in AD, one of our exosome-application interests in therapy [2, 100]. Our results showed that miR-124-3p and miR-146a-5p tend to increase in undifferentiated SH-*WT* neuroblastoma cells and ReN cells as compared to differentiated ones, without changes in miR-155-5p, miR-21-5p and miR-125b-5p. In addition, miRNA cargo in bioreactor-derived exosomes, mainly in those from DASbox-expanded ReN cells, also evidence a small increase for miR-124-3p, miR-146a-5p and miR-125b-5p. Previous studies have shown that variability on miRNA abundance depend on the cell sources [57, 61], that miRNAs likely decline with differentiation [101] and that the miRNA cargo is promoted in exosomes from the bioreactor culture [24], in line with our data. However, further studies are necessary on these issues considering the relevance of exosomes as miRNA carriers.

A key factor in using exosomes as drug delivery vehicles is their ability to uptake and deliver molecules [102, 103], including miRNAs that modulate the inflammatory responses [99]. Among the several hit inflammatory miRNAs, we chose miR-124-3p because it is the most predominant in the adult brain [104] and one of the most involved in the regulation of neuron-microglia paracrine signaling and neuroprotective mechanisms [2]. Its enrichment in exosomes were previously used for diseases such as Huntington's [64] and Parkinson's [31]. There are several ways for loading miRNAs into exosomes and in a five-method comparative study, the ExoFect kit had the highest efficiency [105]. In conformity, this was our method of choice to load pre-miR-124-3p in exosomes from 2D and 3D bioreactor cultures to examine if ReN cell growth conditions affected exosome transfection. As far as we know we were pioneer in such evaluation. Exosomes from the DASbox bioreactor showed superior transfection efficiency, suggesting enhanced cargo incorporation of miR-124-3p, consistent with the known interactions between ExoFect and exosomal membranes [105].

Exosomal internalization and cargo release into the target cells are key for therapeutic efficacy [79, 106]. Our data pointed to DASbox bioreactor upscaled ReN cell-derived exosomes as the better approach to obtain higher microglial miR-124-3p levels that can derive either from increased exosome recognition or inducible effects. We hypothesize that subtle differences in membrane lipid composition, potentially influenced by culture conditions, may contribute to the observed variations in loading efficiency. For instance, cholesterol depletion favors EVs uptake in glial cells, which may derive from changes in plasma membrane fluidity [107]. These biological membrane characteristics, along with membrane protein dynamics, play a crucial role in regulating cell-to-cell communication and initiating intracellular signaling [108]. Future studies will explore these characteristics in the miRNA-124-3p engineered exosomes from bioreactor-expanded ReN cells using lipidomics and proteomics.

Exosome-based therapies require adherence to specific pharmacological guidelines (e.g., formulation and function, efficacy, activity, therapeutic capacity and safety), which must be validated through in vitro and in vivo tests [109]. Confirming the neuronal miR-124-3p preferential expression [110], our data confirmed its increased levels in SH-*WT* and SH-*SWE* cells, relatively to glial cells, mainly to microglia, as we noticed before [38]. We have previously shown that the treatment of these cells with a low dose of H_2O_2 reduces the expression of miR-124-3p [2], a trend that we also observed in the present study. Addition of miR-124 enriched exosomes did not significantly change its expression, probably due to the elevated levels that the naïve cells already present (i.e., neurons show a 3000-fold increase in miR-124 vs. microglia) [111]. However, when considering the expression of STAT3, a key regulator of inflammation and immunogenicity [112], we noticed that the miR-124-loaded exosomes caused its significant reduction in the SH-*WT* cells and non-H_2O_2 treated SH-*SWE* cells. Previous studies demonstrated that targeting STAT3 in AD inhibits neuroinflammation [75] validating the potential anti-inflammatory role of our pre-miR-124-3p engineered exosomes.

As astrocytes and microglia are the main cells implicated in brain inflammation, we then tested our potentially therapeutic exosomes in these cells without and with stimulation. Therefore, we used a stressed cytokine cocktail (IL1α/TNFα/C1q) proposed to induce the expression of inflammatory mediators in astrocytes [73]. Though not significant, we observed an elevation of miR-124-3p in cells treated with miR-124-exosomes when compared to the addition of naïve exosomes, independently of the activation of the IM-HA astrocytes. Intriguingly, if analyzing the effects on the gene expression of FABP7, we noticed its elevation by the naïve exosomes on the stimulated astrocytes and by the pre-miR-124-3p engineered exosomes in either stimulated or non-stimulated cells. Some studies associate FABP7 with an inflammatory response in astrocytes [113, 114], while others propose an inhibitory role [76, 115]. Such controversy deserves further studies, but we may anticipate that it can be a protective and adaptive response of astrocytes to stress-induced inflammation, instead of being pathological by itself, what would indicate the beneficial role of our pre-miR-124-3p engineered exosomes. Indeed,

it was shown that the transfer of miR-124-3p from neuron to astrocytes and microglia, mediated by exosomes, suppresses the activation of neurotoxic astrocytes and microglia in the injured spinal cord [116]. Actually, Ponomarev et al. have demonstrated that miR-124 is a key regulator of microglia homeostasis [28]. CHME3 microglia revealed significantly increased expression of miR-124 after the addition of the exosomes enriched with miR-124, independently of the activation treatment (though the upregulation was not so pronounced in the stressed cells), as compared to non-treated cells or naïve exosomes-treated cells. Moreover, it was reflected in protection of RAGE expression, mainly under activated conditions, which was shown to prevent inflammatory neurodegeneration [117, 118]. Overall, exosome internalization resulted in the regulation of miR-124 and its targets, ameliorating the cell biological function, though variations occurred with the cell type and condition, emphasizing the need for tailored therapeutic strategies in exosome-based interventions.

The results presented in this study provide novel and relevant insights into the scalable production and therapeutic potential of NSC-derived exosomes, although we cannot obviate certain limitations. First, while we demonstrate promising cellular responses to miR-124-3p-loaded exosomes, a deeper mechanistic understanding, particularly through transcriptomic and proteomic profiling, is necessary to elucidate the specific downstream pathways modulated in each recipient cell type. Second, although NSC-derived exosomes are generally associated with low immunogenicity, their potential interactions with the host immune system, especially under conditions of repeated or systemic administration, warrant thorough investigation. Third, exosome therapeutic effects are based on in vitro models which, although highly controlled and informative, cannot fully replicate the complexity of the in vivo brain environment. Finally, since our isolation protocol enriches for sEVs, which was our objective, the heterogeneity of vesicles secreted by NPC aggregates was not addressed this time, though upcoming work should evaluate the effects of shear stress on EV composition and size. In future preclinical studies these issues must be evaluated once they are critical for clinical translation. Therefore, next studies will focus on integrating omics technologies, refining in vivo models, and addressing the immunogenicity of exosomes to fully elucidate their clinical potential. Despite these limitations, our findings establish a strong foundation for the development of exosome-based miR-124-3p therapy and open new avenues for scalable, cell-free interventions for detrimental neuroinflammation in neurodegenerative diseases.

Conclusions

Our findings demonstrate that ReN cells, derived from the ventral mesencephalon of the human fetal brain, retain essential stem cell properties when cultured as neurospheres in bioreactors. Additionally, our work highlights the scalability of exosomes derived from ReN neurospheres produced in the DASbox bioreactor, showcasing their advantages (consistent size and miRNA load) over both static cultures and the PBS 0.1 Mini vertical-wheel bioreactor. This stability suggests that exosome biogenesis remains preserved across different growth conditions, a key factor for therapeutic applications. Notably, DASbox-derived exosomes exhibited superior transfection efficiency with pre-miR-124-3p and showed enhanced internalization by microglial cells, likely due to culture-induced variations in the membrane lipid composition, making them prime candidates for a potential therapeutic approach. Moreover, the uptake of the DASbox-miR-124-3p exosomes also occurs by the target cells, though at a lower level in neurons and astrocytes than in microglia, where they regulate inflammatory mediators, potentially exerting neuroprotective benefits and reestablishing neuron-glia homeostasis. These results underscore the importance of optimizing exosome production to ensure high quality and efficacy for clinical applications. As exosome-based therapies advance, our findings pave the way for further advancements in miRNA therapeutic delivery strategies in regenerative medicine, offering a promising strategy for targeted small molecule delivery and gene regulation. By addressing the challenges associated with exosome production and enhancing their therapeutic potential with miR-124-3p loading, we contribute to the growing body of knowledge necessary for the successful integration of exosome technologies in the clinical practice of neurodegenerative diseases requiring immunoregulatory strategies.

Abbreviations

AB/AM	Antibiotic/antimycotic
AD	Alzheimer's disease
APP	Amyloid precursor protein
BACE1	Beta-secretase 1
C1q	C1 convertase
DAPI	4',6'-diamino-2-fenil-indol
DMEM	Dulbecco's Modified Eagle's Medium
DPBS	Dulbecco's Phosphate-Buffered Saline
EGF	Epidermal growth factor
Exos	Exosomes
EVs	Extracellular vesicles
FABP7	Fatty acid binding protein 7
FBS	Fetal bovine serum
FGF	Fibroblast growth factor
GFAP	Glial fibrillary acid protein
H_2O_2	Hydrogen peroxide
IFN-γ	Interferon gamma
IL-1α	Interleukin 1-alpha
IM-HA	Human immortalized astrocyte cell line
iPSCs	Induced pluripotential stem cells
miR-/miRNA	microRNA
MISEV	Minimal information for studies of extracellular vesicles

MSCs	Mesenchymal stem cells
NPCs	Neural precursor cells
NSCs	Neural stem cells
NTA	Nanoparticle tracking analysis
P/S	Penicillin/streptomycin
RAGE	Receptor for advanced glycation end products
RPL18	Ribosomal protein L18
RT	Room temperature
SEM	Standard error of the mean
sEV	Small extracellular vesicles
Sox2	SRY-Box transcription factor 2
STAT3	Signal transducer and activator of transcription 3
TBS	Tris-Buffer Saline
TNF-α	Tumor necrosis factor alpha

Acknowledgements
We thank BioRender.com for providing the platform used to create some of the scientific illustrations included in this manuscript. Such Figures were created with BioRender and are included with permission.

Author contributions
MC-G: data curation; formal analysis, investigation, methodology, visualization, writing–original draft, software, supervision, and validation; MI: investigation, methodology, validation, visualization, software and writing–original draft; DN: investigation, methodology; WS: investigation, methodology; MM: investigation, methodology; MG-A: resources; CR: investigation, methodology, resources, project administration; supervision, writing–original draft; JC: Resources; DB: conceptualization, data curation; formal analysis; funding acquisition; investigation; project administration; resources, supervision, validation, visualization, writing–review and editing.

Funding
This work was funded by Fundação para a Ciência e a Tecnologia (FCT) (PTDC/MED-NEU/2382/2021) to DB, UID/04138/2025 to the Research Institute for Medicines of the Faculdade de Farmácia, Universidade de Lisboa (Med. ULisboa), UID/04565/2025 to iBB and LA/P/0140/2020 to i4HB. This work was also funded by the Spanish Ministry of Universities (University of Valladolid) - CONVREC-2022-58 and Margarita Salas postdoctoral grant to MCG, as well as by Ministerio de Ciencia e Innovacion y Universidades – Proyectos de Generación de Conocimiento (PID2024-160890OB-I00) and Consejeria de Universidad, Investigacion e Innovacion de la Junta de Andalucia (FEDER-UCA-2024-A2-10) to MGA. MI received support through an Erasmus+ grant from the Università degli Studi di Trieste for her master thesis in DB laboratory.

Data availability
Data will be made available on request.

Declarations

Ethics approval and consent to participate
Not applicable.

Consent for publication
Not applicable.

Competing interests
The authors declare no competing interests.

Author details
[1]Neuroinflammation Signaling and Neuroregeneration, Research Institute for Medicines (iMed.ULisboa), Faculdade de Farmácia, Universidade de Lisboa, Lisbon, Portugal
[2]Division of Physiology, School of Medicine, Universidad de Cadiz, Cadiz, Spain
[3]Dipartimento di Scienze della Vita, Università degli Studi di Trieste, Trieste, Italy
[4]Department of Bioengineering, iBB - Institute for Bioengineering and Biosciences and Associate Laboratory i4HB - Institute for Health and Bioeconomy, Instituto Superior Técnico, Universidade de Lisboa, Lisbon, Portugal
[5]ISEL - Instituto Superior de Engenharia de Lisboa, Instituto Politécnico de Lisboa, Lisbon, Portugal
[6]Biomedical Research and Innovation Institute of Cadiz (INiBICA), Hospital Universitario Puerta del Mar, Cadiz, Spain
[7]iCell4Food, Matosinhos, Portugal
[8]Department of Pharmaceutical Sciences and Medicines, Faculdade de Farmácia, Universidade de Lisboa, Lisbon, Portugal

Received: 3 August 2025 / Accepted: 8 December 2025
Published online: 19 February 2026

References

1. Welsh JA, Goberdhan DCI, O'Driscoll L, Buzas EI, Blenkiron C, Bussolati B, et al. Minimal information for studies of extracellular vesicles (MISEV2023): from basic to advanced approaches. J Extracell Vesicles. 2024;13(2):e12404. https://doi.org/10.1002/jev2.12404.
2. Évora A, Garcia G, Rubi A, De Vitis E, Matos AT, Vaz AR, et al. Exosomes enriched with miR-124-3p show therapeutic potential in a new microfluidic triculture model that recapitulates neuron–glia crosstalk in Alzheimer's disease. Front Pharmacol. 2025;16. https://doi.org/10.3389/fphar.2025.1474012.
3. Zhou X, Huang J, Zhang D, Qian Z, Zuo X, Sun Y. Small extracellular vesicles: the origins, current status, future prospects, and applications. Stem Cell Res Ther. 2025;16(1):184. https://doi.org/10.1186/s13287-025-04330-5.
4. Loch-Neckel G, Matos AT, Vaz AR, Brites D. Challenges in the development of drug delivery systems based on small extracellular vesicles for therapy of brain diseases. Front Pharmacol. 2022;13:839790. https://doi.org/10.3389/fphar.2022.839790.
5. Song Y, Kim Y, Ha S, Sheller-Miller S, Yoo J, Choi C, et al. The emerging role of exosomes as novel therapeutics: Biology, technologies, clinical applications, and the next. Am J Reprod Immunol. 2021;85(2):e13329. https://doi.org/10.1111/aji.13329.
6. Li X, Zhu Y, Wang Y, Xia X, Zheng JC. Neural stem/progenitor cell-derived extracellular vesicles: a novel therapy for neurological diseases and beyond. MedComm (2020). 2023;4(1):e214. https://doi.org/10.1002/mco2.214.
7. De Gioia R, Biella F, Citterio G, Rizzo F, Abati E, Nizzardo M, et al. Neural stem cell transplantation for neurodegenerative diseases. Int J Mol Sci. 2020;21(9). https://doi.org/10.3390/ijms21093103.
8. Hayashi Y, Lin HT, Lee CC, Tsai KJ. Effects of neural stem cell transplantation in alzheimer's disease models. J Biomed Sci. 2020;27(1):29. https://doi.org/10.1186/s12929-020-0622-x.
9. Rhee YH, Kim TH, Jo AY, Chang MY, Park CH, Kim SM, et al. LIN28A enhances the therapeutic potential of cultured neural stem cells in a parkinson's disease model. Brain. 2016;139(Pt 10):2722–39. https://doi.org/10.1093/brain/aww203.
10. Zhang WM, Zhang ZR, Yang XT, Zhang YG, Gao YS. Overexpression of miR–21 promotes neural stem cell proliferation and neural differentiation via the Wnt/beta–catenin signaling pathway in vitro. Mol Med Rep. 2018;17(1):330–5. https://doi.org/10.3892/mmr.2017.7856.
11. Kalluri R, LeBleu VS. The biology, function, and biomedical applications of exosomes. Science. 2020;367(6478). https://doi.org/10.1126/science.aau6977.
12. Noori L, Arabzadeh S, Mohamadi Y, Mojaverrostami S, Mokhtari T, Akbari M, et al. Intrathecal administration of the extracellular vesicles derived from human wharton's jelly stem cells inhibit inflammation and attenuate the activity of inflammasome complexes after spinal cord injury in rats. Neurosci Res. 2021;170:87–98. https://doi.org/10.1016/j.neures.2020.07.011.
13. Fayazi N, Sheykhhasan M, Soleimani Asl S, Najafi R. Stem Cell-Derived exosomes: a new strategy of neurodegenerative disease treatment. Mol Neurobiol. 2021;58(7):3494–514. https://doi.org/10.1007/s12035-021-02324-x.
14. Tan F, Li X, Wang Z, Li J, Shahzad K, Zheng J. Clinical applications of stem cell-derived exosomes. Signal Transduct Target Ther. 2024;9(1):17. https://doi.org/10.1038/s41392-023-01704-0.
15. Yuan P, Ding L, Chen H, Wang Y, Li C, Zhao S, et al. Neural stem cell-derived exosomes regulate neural stem cell differentiation through miR-9-Hes1 axis. Front Cell Dev Biol. 2021;9:601600. https://doi.org/10.3389/fcell.2021.601600.
16. Syromiatnikova V, Prokopeva A, Gomzikova M. Methods of the large-scale production of extracellular vesicles. Int J Mol Sci. 2022;23(18). https://doi.org/10.3390/ijms231810522.

17. Borys BS, Dang T, So T, Rohani L, Revay T, Walsh T, et al. Overcoming bioprocess bottlenecks in the large-scale expansion of high-quality HiPSC aggregates in vertical-wheel stirred suspension bioreactors. Stem Cell Res Ther. 2021;12(1):55. https://doi.org/10.1186/s13287-020-02109-4.
18. Nogueira DES, Rodrigues CAV, Carvalho MS, Miranda CC, Hashimura Y, Jung S, et al. Strategies for the expansion of human induced pluripotent stem cells as aggregates in single-use Vertical-Wheel bioreactors. J Biol Eng. 2019;13:74. https://doi.org/10.1186/s13036-019-0204-1.
19. Dang T, Borys BS, Kanwar S, Colter J, Worden H, Blatchford A, et al. Computational fluid dynamic characterization of vertical-wheel bioreactors used for effective scale-up of human induced pluripotent stem cell aggregate culture. Can J Chem Eng. 2021;99(11):2536–53. https://doi.org/10.1002/cjce.24253.
20. Gomes CM, Sebastiao MJ, Silva G, Moura F, Simao D, Gomes-Alves P, et al. Miniaturization of hiPSC-derived 3D neural cultures in stirred-tank bioreactors for parallelized preclinical assessment of rAAV. Front Bioeng Biotechnol. 2024;12:1379597. https://doi.org/10.3389/fbioe.2024.1379597.
21. Lakshman N, Bourget C, Siu R, Bamm VV, Xu W, Harauz G, et al. Niche-dependent Inhibition of neural stem cell proliferation and oligodendrogenesis is mediated by the presence of Myelin basic protein. Stem Cells. 2021;39(6):776–86. https://doi.org/10.1002/stem.3344.
22. Yan Y, Song L, Tsai AC, Ma T, Li Y. Generation of neural progenitor spheres from human pluripotent stem cells in a suspension bioreactor. Methods Mol Biol. 2016;1502:119–28. https://doi.org/10.1007/7651_2015_310.
23. Manstein F, Ullmann K, Triebert W, Zweigerdt R. Process control and in Silico modeling strategies for enabling high density culture of human pluripotent stem cells in stirred tank bioreactors. STAR Protoc. 2021;2(4):100988. https://doi.org/10.1016/j.xpro.2021.100988.
24. Jeske R, Liu C, Duke L, Canonicco Castro ML, Muok L, Arthur P, et al. Upscaling human mesenchymal stromal cell production in a novel vertical-wheel bioreactor enhances extracellular vesicle secretion and cargo profile. Bioact Mater. 2023;25:732–47. https://doi.org/10.1016/j.bioactmat.2022.07.004.
25. Oveili E, Vafaei S, Bazavar H, Eslami Y, Mamaghanizadeh E, Yasamineh S, et al. The potential use of mesenchymal stem cells-derived exosomes as MicroRNAs delivery systems in different diseases. Cell Commun Signal. 2023;21(1):20. https://doi.org/10.1186/s12964-022-01017-9.
26. Garcia G, Fernandes A, Stein F, Brites D. Protective signature of IFNgamma-Stimulated microglia relies on miR-124-3p regulation from the secretome released by mutant APP Swedish neuronal cells. Front Pharmacol. 2022;13:833066. https://doi.org/10.3389/fphar.2022.833066.
27. Garcia G, Pinto S, Cunha M, Fernandes A, Koistinaho J, Brites D. Neuronal dynamics and miRNA signaling differ between SH-SY5Y APPSwe and PSEN1 mutant iPSC-derived AD models upon modulation with miR-124 mimic and inhibitor. Cells. 2021;10(9). https://doi.org/10.3390/cells10092424.
28. Ponomarev ED, Veremeyko T, Barteneva N, Krichevsky AM, Weiner HL. MicroRNA-124 promotes microglia quiescence and suppresses EAE by deactivating macrophages via the C/EBP-alpha-PU.1 pathway. Nat Med. 2011;17(1):64–70. https://doi.org/10.1038/nm.2266.
29. Du X, Huo X, Yang Y, Hu Z, Botchway BOA, Jiang Y, et al. miR-124 downregulates BACE 1 and alters autophagy in APP/PS1 Transgenic mice. Toxicol Lett. 2017;280:195–205. https://doi.org/10.1016/j.toxlet.2017.08.082.
30. Kang Q, Xiang Y, Li D, Liang J, Zhang X, Zhou F, et al. MiR-124-3p attenuates hyperphosphorylation of Tau protein-induced apoptosis via caveolin-1-PI3K/Akt/GSK3beta pathway in N2a/APP695swe cells. Oncotarget. 2017;8(15):24314–26. https://doi.org/10.18632/oncotarget.15149.
31. Esteves M, Abreu R, Fernandes H, Serra-Almeida C, Martins PAT, Barao M, et al. MicroRNA-124-3p-enriched small extracellular vesicles as a therapeutic approach for parkinson's disease. Mol Ther. 2022;30(10):3176–92. https://doi.org/10.1016/j.ymthe.2022.06.003.
32. Zhong L, Wang J, Wang P, Liu X, Liu P, Cheng X, et al. Neural stem cell-derived exosomes and regeneration: cell-free therapeutic strategies for traumatic brain injury. Stem Cell Res Ther. 2023;14(1):198. https://doi.org/10.1186/s13287-023-03409-1.
33. Hoang DH, Nguyen TD, Nguyen HP, Nguyen XH, Do PTX, Dang VD, et al. Differential wound healing capacity of mesenchymal stem Cell-Derived exosomes originated from bone Marrow, adipose tissue and umbilical cord under Serum- and Xeno-Free condition. Front Mol Biosci. 2020;7:119. https://doi.org/10.3389/fmolb.2020.00119.
34. Qing L, Chen H, Tang J, Jia X. Exosomes and their MicroRNA cargo: new players in peripheral nerve regeneration. Neurorehabil Neural Repair. 2018;32(9):765–76. https://doi.org/10.1177/1545968318798955.
35. Oblak AL, Lin PB, Kotredes KP, Pandey RS, Garceau D, Williams HM, et al. Comprehensive evaluation of the 5XFAD mouse model for preclinical testing applications: A MODEL-AD study. Front Aging Neurosci. 2021;13:713726. https://doi.org/10.3389/fnagi.2021.713726.
36. Donato R, Miljan EA, Hines SJ, Aouabdi S, Pollock K, Patel S, et al. Differential development of neuronal physiological responsiveness in two human neural stem cell lines. BMC Neurosci. 2007;8:36. https://doi.org/10.1186/1471-2202-8-36.
37. Pinto S, Cunha C, Barbosa M, Vaz AR, Brites D. Exosomes from NSC-34 cells transfected with hSOD1-G93A are enriched in miR-124 and drive alterations in microglia phenotype. Front Neurosci. 2017;11:273. https://doi.org/10.3389/fnins.2017.00273.
38. Garcia G, Pinto S, Ferreira S, Lopes D, Serrador MJ, Fernandes A, et al. Emerging role of miR-21-5p in neuron-glia dysregulation and exosome transfer using multiple models of Alzheimer's disease. Cells. 2022;11(21). https://doi.org/10.3390/cells11213377.
39. Belyaev ND, Kellett KA, Beckett C, Makova NZ, Revett TJ, Nalivaeva NN, et al. The transcriptionally active amyloid precursor protein (APP) intracellular domain is preferentially produced from the 695 isoform of APP in a beta-secretase-dependent pathway. J Biol Chem. 2010;285(53):41443–54. https://doi.org/10.1074/jbc.M110.141390.
40. Janabi N, Peudenier S, Heron B, Ng KH, Tardieu M. Establishment of human microglial cell lines after transfection of primary cultures of embryonic microglial cells with the SV40 large T antigen. Neurosci Lett. 1995;195(2):105–8. https://doi.org/10.1016/0304-3940(94)11792-h.
41. Shelke GV, Lasser C, Gho YS, Lotvall J. Importance of exosome depletion protocols to eliminate functional and RNA-containing extracellular vesicles from fetal bovine serum. J Extracell Vesicles. 2014;3. https://doi.org/10.3402/jev.v3.24783.
42. Lehrich BM, Liang Y, Fiandaca MS. Foetal bovine serum influence on in vitro extracellular vesicle analyses. J Extracell Vesicles. 2021;10(3):e12061. https://doi.org/10.1002/jev2.12061.
43. Schurz M, Danmayr J, Jaritsch M, Klinglmayr E, Benirschke HM, Matea CT, et al. EVAnalyzer: high content imaging for rigorous characterisation of single extracellular vesicles using standard laboratory equipment and a new open-source ImageJ/Fiji plugin. J Extracell Vesicles. 2022;11(12):e12282. https://doi.org/10.1002/jev2.12282.
44. Livak KJ, Schmittgen TD. Analysis of relative gene expression data using real-time quantitative PCR and the 2(-Delta delta C(T)) method. Methods. 2001;25(4):402–8. https://doi.org/10.1006/meth.2001.1262.
45. Kolde R. pheatmap: Pretty Heatmaps. [Internet]. [cited 2025 Dec 13]. Available from: https://github.com/raivokolde/pheatmap.
46. Chernyshev VS, Rachamadugu R, Tseng YH, Belnap DM, Jia Y, Branch KJ, et al. Size and shape characterization of hydrated and desiccated exosomes. Anal Bioanal Chem. 2015;407(12):3285–301. https://doi.org/10.1007/s00216-015-8535-3.
47. Kink JA, Bellio MA, Forsberg MH, Lobo A, Thickens AS, Lewis BM, et al. Large-scale bioreactor production of extracellular vesicles from mesenchymal stromal cells for treatment of acute radiation syndrome. Stem Cell Res Ther. 2024;15(1):72. https://doi.org/10.1186/s13287-024-03688-2.
48. Fernandes A, Ribeiro AR, Monteiro M, Garcia G, Vaz AR, Brites D. Secretome from SH-SY5Y APP(Swe) cells trigger time-dependent CHME3 microglia activation phenotypes, ultimately leading to miR-21 exosome shuttling. Biochimie. 2018;155:67–82. https://doi.org/10.1016/j.biochi.2018.05.015.
49. Yin K, Wang S, Zhao RC. Exosomes from mesenchymal stem/stromal cells: a new therapeutic paradigm. Biomark Res. 2019;7:8. https://doi.org/10.1186/s40364-019-0159-x.
50. Graham V, Khudyakov J, Ellis P, Pevny L. SOX2 functions to maintain neural progenitor identity. Neuron. 2003;39(5):749–65. https://doi.org/10.1016/s0896-6273(03)00497-5.
51. Thomson M, Liu SJ, Zou LN, Smith Z, Meissner A, Ramanathan S. Pluripotency factors in embryonic stem cells regulate differentiation into germ layers. Cell. 2011;145(6):875–89. https://doi.org/10.1016/j.cell.2011.05.017.
52. Chen HL, Yuh CH, Wu KK. Nestin is essential for zebrafish brain and eye development through control of progenitor cell apoptosis. PLoS ONE. 2010;5(2):e9318. https://doi.org/10.1371/journal.pone.0009318.
53. Fanarraga M, Avila J, Zabala J. Expression of unphosphorylated class III beta-tubulin isotype in neuroepithelial cells demonstrates neuroblast commitment and differentiation. Eur J Neurosci. 1999;11(2):516–27.
54. Fiock KL, Smalley ME, Crary JF, Pasca AM, Hefti MM. Increased Tau expression correlates with neuronal maturation in the developing human cerebral cortex. eNeuro. 2020;7(3). https://doi.org/10.1523/ENEURO.0058-20.2020.

55. Cunha C, Gomes C, Vaz AR, Brites D. Exploring new inflammatory biomarkers and pathways during LPS-Induced M1 polarization. Mediators Inflamm. 2016;2016:6986175. https://doi.org/10.1155/2016/6986175.
56. Brites D. Regulatory function of microRNAs in microglia. Glia. 2020;68(8):1631–42. https://doi.org/10.1002/glia.23846.
57. Yu X, Odenthal M, Fries JW. Exosomes as miRNA carriers: Formation-function-future. Int J Mol Sci. 2016;17(12). https://doi.org/10.3390/ijms17122028.
58. Qi L, Zhang Y. The MicroRNA 132 regulates fluid shear stress-induced differentiation in periodontal ligament cells through mTOR signaling pathway. Cell Physiol Biochem. 2014;33(2):433–45. https://doi.org/10.1159/000358624.
59. Li CX, Talele NP, Boo S, Koehler A, Knee-Walden E, Balestrini JL, et al. MicroRNA-21 preserves the fibrotic mechanical memory of mesenchymal stem cells. Nat Mater. 2017;16(3):379–89. https://doi.org/10.1038/nmat4780.
60. Ferguson S, Kim S, Lee C, Deci M, Nguyen J. The phenotypic effects of exosomes secreted from distinct cellular sources: a comparative study based on miRNA composition. AAPS J. 2018;20(4):67. https://doi.org/10.1208/s12248-018-0227-4.
61. Soni N, Gupta S, Rawat S, Krishnakumar V, Mohanty S, Banerjee A. microRNA-enriched exosomes from different sources of mesenchymal stem cells can differentially modulate functions of immune cells and neurogenesis. Biomedicines. 2021;10(1). https://doi.org/10.3390/biomedicines10010069.
62. Yang J, Zhang X, Chen X, Wang L, Yang G. Exosome mediated delivery of miR-124 promotes neurogenesis after ischemia. Mol Ther Nucleic Acids. 2017;7:278–87. https://doi.org/10.1016/j.omtn.2017.04.010.
63. Mavroudis I, Balmus IM, Ciobica A, Nicoara MN, Luca AC, Palade DO. The role of microglial exosomes and miR-124-3p in neuroinflammation and neuronal repair after traumatic brain injury. Life (Basel). 2023;13(9). https://doi.org/10.3390/life13091924.
64. Lee ST, Im W, Ban JJ, Lee M, Jung KH, Lee SK, et al. Exosome-Based delivery of miR-124 in a huntington's disease model. J Mov Disord. 2017;10(1):45–52. https://doi.org/10.14802/jmd.16054.
65. Ge X, Guo M, Hu T, Li W, Huang S, Yin Z, et al. Increased microglial Exosomal miR-124-3p alleviates neurodegeneration and improves cognitive outcome after RmTBI. Mol Ther. 2020;28(2):503–22. https://doi.org/10.1016/j.ymthe.2019.11.017.
66. VanRyzin JW. Phagocytic microglia in development: are they what they eat? Brain Behav Immun Health. 2021;18:100373. https://doi.org/10.1016/j.bbih.2021.100373.
67. Men Y, Yelick J, Jin S, Tian Y, Chiang MSR, Higashimori H, et al. Exosome reporter mice reveal the involvement of exosomes in mediating neuron to astroglia communication in the CNS. Nat Commun. 2019;10(1):4136. https://doi.org/10.1038/s41467-019-11534-w.
68. Paolicelli RC, Bergamini G, Rajendran L. Cell-to-cell communication by extracellular vesicles: focus on microglia. Neuroscience. 2019;405:148–57. https://doi.org/10.1016/j.neuroscience.2018.04.003.
69. Akbari-Gharalari N, Khodakarimi S, Nezhadshahmohammad F, Karimipour M, Ebrahimi-Kalan A, Wu J. Exosomes in neuron-glia communication: A review on neurodegeneration. Bioimpacts. 2024;14(5):30153. https://doi.org/10.34172/bi.2023.30153.
70. Chen L, Xiong Y, Chopp M, Zhang Y. Engineered exosomes enriched with select MicroRNAs amplify their therapeutic efficacy for traumatic brain injury and stroke. Front Cell Neurosci. 2024;18:1376601. https://doi.org/10.3389/fncel.2024.1376601.
71. Saikia B, Dhanushkodi A. Engineered exosome therapeutics for neurodegenerative diseases. Life Sci. 2024;356:123019. https://doi.org/10.1016/j.lfs.2024.123019.
72. Chadwick W, Zhou Y, Park SS, Wang L, Mitchell N, Stone MD, et al. Minimal peroxide exposure of neuronal cells induces multifaceted adaptive responses. PLoS ONE. 2010;5(12):e14352. https://doi.org/10.1371/journal.pone.0014352.
73. Liddelow SA, Guttenplan KA, Clarke LE, Bennett FC, Bohlen CJ, Schirmer L, et al. Neurotoxic reactive astrocytes are induced by activated microglia. Nature. 2017;541(7638):481–7. https://doi.org/10.1038/nature21029.
74. Kang YJ, Hyeon SJ, McQuade A, Lim J, Baek SH, Diep YN, et al. Neurotoxic microglial activation via IFNgamma-Induced Nrf2 reduction exacerbating alzheimer's disease. Adv Sci (Weinh). 2024;11(20):e2304357. https://doi.org/10.1002/advs.202304357.
75. Wen X, Hu J. Targeting STAT3 signaling pathway in the treatment of alzheimer's disease with compounds from natural products. Int Immunopharmacol. 2024;141:112936. https://doi.org/10.1016/j.intimp.2024.112936.
76. Kamizato K, Sato S, Shil SK, Umaru BA, Kagawa Y, Yamamoto Y, et al. The role of fatty acid binding protein 7 in spinal cord astrocytes in a mouse model of experimental autoimmune encephalomyelitis. Neuroscience. 2019;409:120–9. https://doi.org/10.1016/j.neuroscience.2019.03.050.
77. MacLean M, Juranek J, Cuddapah S, Lopez-Diez R, Ruiz HH, Hu J, et al. Microglia RAGE exacerbates the progression of neurodegeneration within the SOD1(G93A) murine model of amyotrophic lateral sclerosis in a sex-dependent manner. J Neuroinflammation. 2021;18(1):139. https://doi.org/10.1186/s12974-021-02191-2.
78. Sbai O, Djelloul M, Auletta A, Ieraci A, Vascotto C, Perrone L. AGE-TXNIP axis drives inflammation in alzheimer's by targeting Abeta to mitochondria in microglia. Cell Death Dis. 2022;13(4):302. https://doi.org/10.1038/s41419-022-04758-0.
79. Gurung S, Perocheau D, Touramanidou L, Baruteau J. The exosome journey: from biogenesis to uptake and intracellular signalling. Cell Commun Signal. 2021;19(1):47. https://doi.org/10.1186/s12964-021-00730-1.
80. Hade MD, Suire CN, Suo Z. Mesenchymal stem cell-derived exosomes: applications in regenerative medicine. Cells. 2021;10(8). https://doi.org/10.3390/cells10081959.
81. Koh HB, Kim HJ, Kang SW, Yoo TH. Exosome-based drug delivery: translation from bench to clinic. Pharmaceutics. 2023;15(8). https://doi.org/10.3390/pharmaceutics15082042.
82. El Andaloussi S, Mager I, Breakefield XO, Wood MJ. Extracellular vesicles: biology and emerging therapeutic opportunities. Nat Rev Drug Discov. 2013;12(5):347–57. https://doi.org/10.1038/nrd3978.
83. Pamulang YV, Oontawee S, Rodprasert W, Padeta I, Sa-Ard-Lam N, Mahanonda R, et al. Potential upscaling protocol establishment and wound healing bioactivity screening of exosomes isolated from canine adipose-derived mesenchymal stem cells. Sci Rep. 2025;15(1):10617. https://doi.org/10.1038/s41598-025-93219-7.
84. Ulpiano C, Salvador W, Franchi-Mendes T, Huang MC, Lin YH, Lin HT, et al. Continuous collection of human mesenchymal-stromal-cell-derived extracellular vesicles from a stirred tank reactor operated under xenogeneic-free conditions for therapeutic applications. Stem Cell Res Ther. 2025;16(1):210. https://doi.org/10.1186/s13287-025-04341-2.
85. Zhang K, Cheng K. Stem cell-derived exosome versus stem cell therapy. Nat Rev Bioeng. 2023;1–2. https://doi.org/10.1038/s44222-023-00064-2.
86. Wang H, Huber CC, Li XP. Mesenchymal and neural stem cell-derived exosomes in treating Alzheimer's disease. Bioeng (Basel). 2023;10(2). https://doi.org/10.3390/bioengineering10020253.
87. Lee KH, Tseng WC, Yang CY, Tarng DC. The anti-inflammatory, anti-oxidative, and anti-apoptotic benefits of stem cells in acute ischemic kidney injury. Int J Mol Sci. 2019;20(14). https://doi.org/10.3390/ijms20143529.
88. Ma Y, Li C, Huang Y, Wang Y, Xia X, Zheng JC. Exosomes released from neural progenitor cells and induced neural progenitor cells regulate neurogenesis through miR-21a. Cell Commun Signal. 2019;17(1):96. https://doi.org/10.1186/s12964-019-0418-3.
89. de Almeida Fuzeta M, Bernardes N, Oliveira FD, Costa AC, Fernandes-Platzgummer A, Farinha JP, et al. Scalable production of human mesenchymal stromal Cell-Derived extracellular vesicles under Serum-/Xeno-Free conditions in a Microcarrier-Based bioreactor culture system. Front Cell Dev Biol. 2020;8:553444. https://doi.org/10.3389/fcell.2020.553444.
90. Haraszti RA, Miller R, Stoppato M, Sere YY, Coles A, Didiot MC, et al. Exosomes produced from 3D cultures of MSCs by tangential flow filtration show higher yield and improved activity. Mol Ther. 2018;26(12):2838–47. https://doi.org/10.1016/j.ymthe.2018.09.015.
91. Palviainen M, Saari H, Karkkainen O, Pekkinen J, Auriola S, Yliperttula M, et al. Metabolic signature of extracellular vesicles depends on the cell culture conditions. J Extracell Vesicles. 2019;8(1):1596669. https://doi.org/10.1080/20013078.2019.1596669.
92. Edmondson R, Broglie JJ, Adcock AF, Yang L. Three-dimensional cell culture systems and their applications in drug discovery and cell-based biosensors. Assay Drug Dev Technol. 2014;12(4):207–18. https://doi.org/10.1089/adt.2014.573.
93. Tejerina S, Dufey V, Hoet JF, Tacheny A, De Longueville F. The DASbox® Mini Bioreactor System as a Tool for Process Development and Stem-Cell Derived Exosome Production in Standardized Culture Conditions. Hamburg, Germany: Eppendorf; 2021.
94. Otahal A, Kramer K, Neubauer M, Gulova S, Lacza Z, Nehrer S, et al. Culture of Hoffa fat pad mesenchymal stem/stromal cells on microcarrier suspension in vertical wheel bioreactor for extracellular vesicle production. Stem Cell Res Ther. 2024;15(1):61. https://doi.org/10.1186/s13287-024-03681-9.

95. Caponnetto F, Manini I, Skrap M, Palmai-Pallag T, Di Loreto C, Beltrami AP, et al. Size-dependent cellular uptake of exosomes. Nanomedicine. 2017;13(3):1011–20. https://doi.org/10.1016/j.nano.2016.12.009.
96. Mourdikoudis S, Pallares RM, Thanh NTK. Characterization techniques for nanoparticles: comparison and complementarity upon studying nanoparticle properties. Nanoscale. 2018;10(27):12871–934. https://doi.org/10.1039/c8nr02278j.
97. Gilbertson JA, Sen A, Behie LA, Kallos MS. Scaled-up production of mammalian neural precursor cell aggregates in computer-controlled suspension bioreactors. Biotechnol Bioeng. 2006;94(4):783–92. https://doi.org/10.1002/bit.20900.
98. Jibing C, Weiping L, Yuwei Y, Bingzheng F, Zhiran X. Exosomal microRNA-Based therapies for skin diseases. Regen Ther. 2024;25:101–12. https://doi.org/10.1016/j.reth.2023.12.005.
99. Alexander M, Hu R, Runtsch MC, Kagele DA, Mosbruger TL, Tolmachova T, et al. Exosome-delivered MicroRNAs modulate the inflammatory response to endotoxin. Nat Commun. 2015;6:7321. https://doi.org/10.1038/ncomms8321.
100. Liang Y, Wang L. Inflamma-MicroRNAs in alzheimer's disease: from disease pathogenesis to therapeutic potentials. Front Cell Neurosci. 2021;15:785433. https://doi.org/10.3389/fncel.2021.785433.
101. Lakshmipathy U, Love B, Goff LA, Jornsten R, Graichen R, Hart RP, et al. MicroRNA expression pattern of undifferentiated and differentiated human embryonic stem cells. Stem Cells Dev. 2007;16(6):1003–16. https://doi.org/10.1089/scd.2007.0026.
102. Herrmann IK, Wood MJA, Fuhrmann G. Extracellular vesicles as a next-generation drug delivery platform. Nat Nanotechnol. 2021;16(7):748–59. https://doi.org/10.1038/s41565-021-00931-2.
103. Kim HI, Park J, Zhu Y, Wang X, Han Y, Zhang D. Recent advances in extracellular vesicles for therapeutic cargo delivery. Exp Mol Med. 2024;56(4):836–49. https://doi.org/10.1038/s12276-024-01201-6.
104. Zhang WH, Jiang L, Li M, Liu J. MicroRNA–124: an emerging therapeutic target in central nervous system disorders. Exp Brain Res. 2023;241(5):1215–26. https://doi.org/10.1007/s00221-022-06524-2.
105. de Abreu RC, Ramos CV, Becher C, Lino M, Jesus C, da Costa Martins PA, et al. Exogenous loading of MiRNAs into small extracellular vesicles. J Extracell Vesicles. 2021;10(10):e12111. https://doi.org/10.1002/jev2.12111.
106. Mulcahy LA, Pink RC, Carter DR. Routes and mechanisms of extracellular vesicle uptake. J Extracell Vesicles. 2014;3. https://doi.org/10.3402/jev.v3.24641.
107. Pantazopoulou M, Lamprokostopoulou A, Karampela DS, Alexaki A, Delis A, Coens A, et al. Differential intracellular trafficking of extracellular vesicles in microglia and astrocytes. Cell Mol Life Sci. 2023;80(7):193. https://doi.org/10.1007/s00018-023-04841-5.
108. Casares D, Escriba PV, Rossello CA. Membrane lipid composition: effect on membrane and organelle structure, function and compartmentalization and therapeutic avenues. Int J Mol Sci. 2019;20(9):2167. https://doi.org/10.3390/ijms20092167.
109. Nguyen VVT, Witwer KW, Verhaar MC, Strunk D, van Balkom BWM. Functional assays to assess the therapeutic potential of extracellular vesicles. J Extracell Vesicles. 2020;10(1):e12033. https://doi.org/10.1002/jev2.12033.
110. Smirnova L, Grafe A, Seiler A, Schumacher S, Nitsch R, Wulczyn FG. Regulation of MiRNA expression during neural cell specification. Eur J Neurosci. 2005;21(6):1469–77. https://doi.org/10.1111/j.1460-9568.2005.03978.x.
111. Wang D, Zhang H, Li M, Frid MG, Flockton AR, McKeon BA, et al. MicroRNA-124 controls the proliferative, migratory, and inflammatory phenotype of pulmonary vascular fibroblasts. Circ Res. 2014;114(1):67–78. https://doi.org/10.1161/CIRCRESAHA.114.301633.
112. Yu H, Pardoll D, Jove R. STATs in cancer inflammation and immunity: a leading role for STAT3. Nat Rev Cancer. 2009;9(11):798–809. https://doi.org/10.1038/nrc2734.
113. Hamilton HL, Kinscherf NA, Balmer G, Bresque M, Salamat SM, Vargas MR, et al. FABP7 drives an inflammatory response in human astrocytes and is upregulated in alzheimer's disease. Geroscience. 2024;46(2):1607–25. https://doi.org/10.1007/s11357-023-00916-0.
114. Killoy KM, Harlan BA, Pehar M, Vargas MR. FABP7 upregulation induces a neurotoxic phenotype in astrocytes. Glia. 2020;68(12):2693–704. https://doi.org/10.1002/glia.23879.
115. Cheng A, Jia W, Kawahata I, Fukunaga K. A novel fatty acid-binding protein 5 and 7 inhibitor ameliorates oligodendrocyte injury in multiple sclerosis mouse models. EBioMedicine. 2021;72:103582. https://doi.org/10.1016/j.ebiom.2021.103582.
116. Jiang D, Gong F, Ge X, Lv C, Huang C, Feng S, et al. Neuron-derived exosomes-transmitted miR-124-3p protect traumatically injured spinal cord by suppressing the activation of neurotoxic microglia and astrocytes. J Nanobiotechnol. 2020;18(1):105. https://doi.org/10.1186/s12951-020-00665-8.
117. Koerich S, Parreira GM, de Almeida DL, Vieira RP, de Oliveira ACP. Receptors for advanced glycation end products (RAGE): promising targets aiming at the treatment of neurodegenerative conditions. Curr Neuropharmacol. 2023;21(2):219–34. https://doi.org/10.2174/1570159X20666220922153903.
118. Derk J, MacLean M, Juranek J, Schmidt AM. The receptor for advanced glycation endproducts (RAGE) and mediation of inflammatory neurodegeneration. J Alzheimers Dis Parkinsonism. 2018;8(1):421. https://doi.org/10.4172/2161-0460.1000421.

Publisher's note

Springer Nature remains neutral with regard to jurisdictional claims in published maps and institutional affiliations.